

國立交通大學

環境工程研究所

博士論文

氣膠微粒在管流中熱泳附著之研究

THERMOPHORETIC DEPOSITION OF AEROSOL
PARTICLES IN TUBE FLOW

研究生：林智賢

指導教授：蔡春進

中華民國九十三年七月

氣膠微粒在管流中熱泳附著之研究

THERMOPHORETIC DEPOSITION OF AEROSOL PARTICLES
IN TUBE FLOW

研究生：林智賢

Student: Jyh-Shyan Lin

指導教授：蔡春進

Advisor: Chuen-Jinn Tsai

國立交通大學

環境工程研究所

博士論文



A Dissertation

Submitted to Institute of Environmental Engineering

College of Engineering

National Chiao Tung University

in Partial Fulfillment of the Requirements

for the Degree of

Doctor of Philosophy

in

Environmental Engineering

July, 2004

Hsinchu, Taiwan, Republic of China

中華民國九十三年七月

摘要

本研究探討管流中微粒的熱泳附著效率。當流場與溫度場皆是在發展狀態時，溫度梯度在圓管進口附近靠近管壁的位置是最高的，微粒的熱泳附著效率可能會增加。因此，本研究首先利用數值模擬的方法探討進口流效應對圓管中微粒熱泳附著效率的影響。而由於 Romay 等人(1998)的紊流熱泳附著效率的實驗值與理論值不合，所以本研究接著用實驗的方法，探討微粒在圓管中的熱泳附著效率並與理論值比對。最後，工業上常用管壁加熱的方法來防止微粒的管壁附著，但是有效防止微粒附著的加熱溫度並未知，因此本研究利用數值模擬及實驗的方法探討微粒在層流圓管中的附著效率。

在發展中的流體對微粒熱泳附著效率影響的研究中，以數值方法來求取微粒在圓管中的臨界軌跡線，藉以計算出對應的熱泳附著效率。研究結果顯示，當流場是完全發展流而溫度場是正在發展中的狀態，微粒的熱泳附著效率只有在圓管進口的位置會稍微高於前述當流場與溫度場皆是完全發展流的案例，然而在 $Z > 5$ 的圓管中，最終的熱泳附著效率會一樣。當流場與溫度場皆是正在發展中的情況時，在 $Z > 5$ 的圓管中，微粒的熱泳附著效率大約是流場與溫度場皆是完全發展流案例的兩倍，而且在進口的位置附著效率會高出甚多。另外，本研究開發出可用在計算層流圓管中，流場與溫度場同時是完全發展流或同時是正在發展中的熱泳附著效率半經驗式。

在層流及紊流圓管的微粒熱泳附著效率實驗中，本研究使用單徑的氯化鈉微粒(微粒粒徑在 0.038 到 0.498 μm 之間)作為測試微粒，用來量測在一長 1.18 公尺，內徑為 0.43 公分圓管中微粒的熱泳附著效率。在 Romay 等人(1998)的研究中，理論的熱泳附著效率和實驗值不合，然而在本研究中，考慮帶有 Boltzmann

靜電平衡微粒的靜電附著、微粒的紊流擴散及慣性衝擊等機制，所以微粒的熱泳附著效率可以準確地被量測出來。

在使用熱泳力來抑制微粒管壁附著這方面，我們將管壁加高溫度使其高於進氣氣流，係利用實驗及數值模擬的方法探討微粒在層流圓管內的附著效率。在數值分析這方面，求解包含熱泳項的對流擴散方程式，求得微粒在圓管內的濃度分佈及附著效率。實驗時使用單徑微粒(微粒粒徑為 0.01, 0.02 and 0.04 μm)作為測試氣膠，量得的實驗值用來驗證數值解。研究結果顯示，微粒的附著效率會隨著管壁溫度的升高或是圓管內氣流量的增加而降低。本研究發展出一個半經驗式可以用來預測在層流圓管中，在給定的無因次附著參數下，求得所需要的無因次溫度差(亦即可求取所需的管壁加熱溫度)來達到零微粒附著效率。



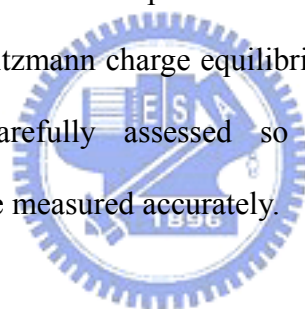
ABSTRACT

This study investigates thermophoretic particle deposition efficiency in a tube flow. The highest temperature gradient near the wall occurs at the entrance of a tube when both flow and temperature are developing, thermophoretic deposition in the entrance region may be enhanced. Therefore, the effect of entrance flow on the thermophoretic deposition efficiency in laminar tube flow was first investigated numerically. In the previous study of Romay et al. (1998), the experimental data don't agree well with theoretical results. In the present study, the thermophoretic particle deposition efficiency in tube flow was studied experimentally and compared with the theoretical predictions. To prevent particle deposition on tube wall, a common practice is to heat up the tube wall in industry. But the required wall temperature to effectively suppress particle deposition in tube wall is unknown. Thus the effect of tube wall temperature on particle deposition efficiency under laminar flow condition was investigated experimentally and numerically.

In the study of developing flow effect in a circular tube on thermophoretic particle deposition efficiency, the critical trajectory method was investigated numerically. The results show that when the flow is fully developed and temperature is developing, it is found that only near the thermal entrance region (or temperature jump region) of the tube the deposition efficiency is slightly higher than the combined fully developed case (flow and temperature), while the deposition efficiency remains the same for $Z > 5$. When both flow and temperature are developing (or combined developing), the deposition efficiency is about twice of the combined fully developed case for $Z > 5$ and is much higher near the entrance of the tube. Non-dimensional equations are developed empirically to predict the thermophoretic deposition

efficiency in combined developing and combined fully developed cases under laminar flow condition.

In the experimental study of thermophoretic deposition of aerosols particles in laminar and turbulent tube flow. Thermophoretic deposition of aerosols particles (particle diameter ranges from 0.038 to 0.498 μm) was measured in a tube (1.18 m long, 0.43 cm inner diameter, stainless-steel tube) using monodisperse NaCl test particles under laminar and turbulent flow conditions. In the previous study by Romay et al. (1998), theoretical thermophoretic deposition efficiencies in turbulent flow regime do not agree well with the experimental data. In this study, particle deposition efficiencies due to other deposition mechanisms such as electrostatic deposition for particles in Boltzmann charge equilibrium, and turbulent diffusion and inertial deposition were carefully assessed so that the deposition due to thermophoresis alone could be measured accurately.



In the aspect of suppression of particle deposition by thermophoretic force, flow through a tube with circular cross section was investigated numerically and experimentally for the case when the wall temperature exceeds that of the gas. Particle transport equations for convection, diffusion and thermophoresis were solved numerically to obtain particle concentration profiles and deposition efficiencies. The numerical results were validated by particle deposition efficiency measurements with monodisperse particles (particle sizes were 0.01, 0.02 and 0.04 μm). For all particle sizes, the particle deposition efficiency was found to decrease with increasing tube wall temperature and gas flow rate. An empirical expression has been developed to predict the dimensionless temperature difference needed for zero deposition efficiency in a laminar tube flow for a given dimensionless deposition parameter.

誌謝

感謝指導教授 蔡春進教授在論文研究期間的殷情指導，使本論文得以完成。特別感謝中央大學 李崇德教授、中興大學 鄭曼婷教授、交通大學 葉弘德教授、白曠綾教授及元智大學 張幼珍教授的指導與協助定稿，使本論文更臻理想。

在研究過程中，實驗室的學弟晉儀、林宏、力群、妮芬、世勳、士軒、開亨、茂銓、思敏、正生、依馨、健倫及已畢業的學弟妹的彼此勉勵與幫忙，使得研究生生活多采多姿。由衷的感謝 江漢全教授，謝謝您在我求學過程中給予最大的協助與幫忙。感謝 張振平博士在論文初期給予的協助。好友世興學長、裕強學長、誌仁、凱文及高中的同窗好友們，謝謝您們在我讀博士期間的加油與精神上的支持。另外，感謝在論文研究期間，當我遇到挫折時鼓勵及幫助我的所有長輩及朋友，謝謝您們。



最後，僅以本文獻予敬愛的爸媽，感謝你們雖然已漸漸年老，仍給予我最大的支持與鼓勵，姐文琪、妹淑華、弟智偉及女友家宜，有了你們一起生活及互相扶持，使我能安心的完成學業，在此將論文獻於您們。

TABLE OF CONTENTS

Abstract (Chinese)	I
Abstract (English)	III
Acknowledgments	V
Table of contents	VI
List of tables	IX
List of figures	X
Nomenclature	XIII
Chapter 1 Introduction	1
1.1 Thermophoretic coefficient and thermophoretic velocity	1
1.2 Thermophoretic deposition efficiency in laminar tube flow	3
1.3 Thermophoretic deposition efficiency in turbulent tube flow	8
1.4 Isothermal particle deposition mechanisms in tube flow	10
1.5 Application of thermophoretic force to suppress particle deposition	15
1.6 Objectives of this study	17
Chapter 2 Numerical methods	18
2.1 Temperature field	18
2.2 Critical particle trajectory method to calculate thermophoretic particle deposition efficiency	22
2.3 Solutions of convection-diffusion equation to obtain thermophoretic particle deposition efficiency	28
Chapter 3 Experimental methods	30
3.1 Aerosol generation and conditioning	30
3.2 Experimental system	33

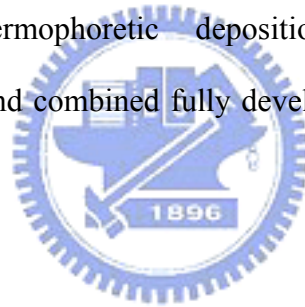
3.3 Experimental procedure	34
Chapter 4 Entrance effect on the thermophoretic deposition efficiency	38
4.1 Thermophoretic deposition efficiency for fully developed temperature and velocity fields	38
4.2 Thermophoretic deposition efficiency for fully developed flow and developing temperature	41
4.3 Thermophoretic deposition efficiency for developing flow and developing temperature	42
4.4 Empirical equation of thermophoretic deposition efficiency for the case of a long tube	48
Chapter 5 Experimental results of the thermophoretic deposition efficiency	51
5.1 Particle deposition efficiency due to isothermal deposition mechanisms	51
5.2 Thermophoretic deposition efficiency	56
Chapter 6 Suppression of particle deposition by thermophoresis	61
6.1 Thermophoretic deposition efficiency for tube wall temperature lower than that of gas flow	61
6.2 Effect of temperature difference between the tube and gas flow on the particle deposition efficiency	64
6.3 Particle deposition efficiency versus dimensionless temperature difference and deposition parameter	67
6.4 An equation to predict the dimensionless temperature difference needed for zero particle deposition	75
6.5 Practical application	76
Chapter 7 Conclusions and future study	77
7.1 Conclusions	77

7.2 Future study	79
Appendix A	81
References	83
Vita	89



LIST OF TABLES

Table 1.1	Theoretical expressions of thermophoretic deposition efficiency for a long tube where the temperature of hot gas has approached that of the wall.	6
Table 1.2	The values of ϕ_0 at different PrK_{th} and θ^* for the short tube case.	6
Table 1.3	The exact solution of Walker et al. (1979) for thermophoretic deposition efficiency in the long tube case.	7
Table 1.4	Theoretical expressions of the thermophoretic deposition efficiency in turbulent tube flow.	9
Table 3.1	Experimental conditions of deposition measurement.	36
Table 3.2	Experimental conditions of suppression measurement.	37
Table 4.1	Accumulated thermophoretic deposition efficiency of combined developing case and combined fully developed case at different positions of a tube.	47



LIST OF FIGURES

Figure 1.1 Fluid element.	9
Figure 2.1 The developing velocity profiles in laminar tube flow.	23
Figure 2.2 Comparison between Graetz's solution and temperature profile in the thermal entry region with that of Grigull and Tratz (1965).	24
Figure 2.3 Critical particle trajectory.	25
Figure 3.1 The schematic diagram of the experimental setup for deposition experiment.	31
Figure 3.2 The schematic diagram of the experimental setup for suppression experiment.	32
Figure 4.1 Comparison of theoretical deposition efficiency with previous theories in laminar tube flow.	39
Figure 4.2 Comparison of present theoretical thermophoretic deposition efficiency with numerical prediction of Stratmann et al. (1994) in laminar tube flow.	40
Figure 4.3 Comparison of accumulated thermophoretic deposition efficiency between different θ^* s versus Z , fully developed flow.	43
Figure 4.4 Dimensionless temperature profiles as a function of dimensionless radial and axial coordinates.	44
Figure 4.5 Accumulated thermophoretic deposition efficiency of aerosol particles using different numbers of grids, combined developing case.	45
Figure 4.6 Comparison of accumulated thermophoretic deposition efficiency between different θ^* s versus Z .	46
Figure 4.7 Thermophoretic deposition efficiency as a function of thermophoretic parameter β_1 in laminar fully developed flow and developing flow.	50

- Figure 5.1 Comparison of experimental deposition efficiencies (isothermal) and theoretical predictions of diffusional and electrostatic deposition under laminar flow conditions, ($Re = 1340$). 52
- Figure 5.2 Comparison of experimental deposition efficiencies (isothermal) and theoretical predictions of combined turbulent diffusion and inertial deposition under turbulent flow conditions ($Re = 6580$). 54
- Figure 5.3 Comparison of experimental data and theoretical predictions of thermophoretic deposition efficiency of combined fully developed case under laminar flow conditions. (a) $Re = 1340$, $T_e = 343$ K (b) $Re = 1340$, $T_e = 373$ K. 55
- Figure 5.4 Comparison of experimental data and theoretical predictions of thermophoretic deposition efficiency of Romay et al. (1998) under turbulent flow conditions. (a) $Re = 6580$, $T_e = 343$ K (b) $Re = 10200$, $T_e = 343$ K. (c) $Re = 10200$, $T_e = 398$ K. 58
- Figure 5.5 Comparison of theoretical predictions ($Re = 10200$) for particles of 0.05 and 0.498 μm in diameter in turbulent flow. 59
- Figure 5.6 Comparison of experimental thermophoretic coefficients K_{th} with theories. Experimental K_{th} is calculated based on experimental data and theoretical thermophoretic deposition efficiency in (a) laminar flow (b) turbulent flow. 60
- Figure 6.1 Particle deposition efficiency as a function of dimensionless parameter, $\mu' = \pi DL/Q$, for isothermal case. 62
- Figure 6.2 Dimensionless temperature profiles as a function of dimensionless radial and axial coordinates. 63

Figure 6.3 Particle deposition efficiency versus tube wall temperature for NaCl particles with particle diameter of (a) 0.01 μm (b) 0.02 μm (c) 0.04 μm . The test tube length and inner diameter are 1.18 and 0.0043 m, respectively, and the inlet air temperature is 296 K. 65

Figure 6.4 Particle deposition efficiency as a function of the dimensionless temperature difference, $T_w/(\text{Pr}K_{\text{th}}(T_w-T_e))$, and deposition parameter, $\pi DL/Q$. Dimensionless deposition parameter is (a) from 1.6×10^{-4} to 1.2×10^{-2} and (b) from 1.2×10^{-2} to 1.16. (Insets in the figures are deposition efficiency curves near zero deposition efficiency. For air and current tube geometry and length, the corresponding wall temperature is marked in the upper x-axis). 70

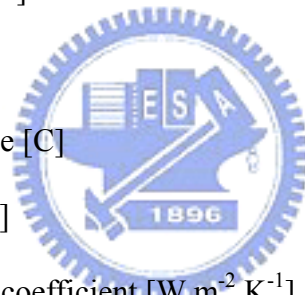
Figure 6.5 The variation of radial particle thermophoretic and diffusional velocities in the axial direction as the tube wall is heated at various temperatures at a given particle diameter of (a) 0.02 μm (b) 0.005 μm and a constant flow rate of 1 l min^{-1} . 71

Figure 6.6 (a) Dimensionless radial concentration profiles and (b) dimensionless radial temperature profiles as a function of dimensionless axial coordinates. The test tube length and inside diameter are 1.18 and 0.0043 m, respectively. 72

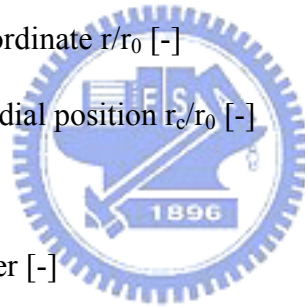
Figure 6.7 The relationship between the required dimensionless temperature difference, $\theta = T_w/(\text{Pr}K_{\text{th}}(T_w-T_e))$, and the dimensionless deposition parameter, $\mu' = \pi DL/Q$, for zero particle deposition for a circular tube air flow. Symbols represent the numerical results and solid line is the fitted curve. 73

NOMENCLATURE

B	dynamic mobility $B = C/3\pi\mu'd_p$ [$\text{m N}^{-1} \text{s}^{-1}$]
c_p	specific heat capacity at constant pressure [$\text{kJ kg}^{-1} \text{K}^{-1}$]
C	slip correction factor [-]
C_d	drag coefficient [-]
C_m	momentum exchange coefficient [-]
C_s	thermal slip coefficient [-]
C_t	temperature jump coefficient [-]
d_p	diameter of the particles [m]
D	particle diffusivity [$\text{m}^2 \text{s}^{-1}$]
D_t	tube diameter [m]
e	elementary unit of charge [C]
f	fanning friction factor [-]
h	convective heat transfer coefficient [$\text{W m}^{-2} \text{K}^{-1}$]
k_g	gas thermal conductivity [$\text{W m}^{-1} \text{K}^{-1}$]
k_p	particle thermal conductivity [$\text{W m}^{-1} \text{K}^{-1}$]
K	Boltzmann constant [N m K^{-1}]
K_E	a constant of proportionality [$\text{N m}^2 \text{C}^{-2}$]
K_{th}	thermophoretic coefficient [-]
L	tube length [m]
m_p	particle mass [kg]
n_p	particle charge [-]
N	particle number concentration [l m^{-3}]
N_e	particle number concentration at inlet [l m^{-3}]



P_d	particle penetration efficiency [-]
$P_{d,\ell}$	diffusional penetration efficiency in laminar tube flow [-]
Pe_g	gas Peclet number $(u_m \cdot r_0^2)/(\alpha \cdot L)$ [-]
Pr	gas Prandtl number [-]
P_{tur}	inertial impaction efficiency in turbulent tube flow [-]
q	the charge on the particle [-]
Q	inlet gas flow rate [$m^3 s^{-1}$]
r	radial coordinate [-]
r_0	tube radius [m]
r_c	critical radial position [m]
R	dimensionless radial coordinate r/r_0 [-]
R_c	dimensionless critical radial position r_c/r_0 [-]
Re	Reynolds number [-]
Re_p	particle Reynolds number [-]
Sc	Schmidt number [-]
t	the elapsed time in the tube [s]
\bar{T}	average temperature of the fluid [K]
T	gas temperature [K]
T_e	gas temperature at tube inlet [K]
T_m	mixing-cup temperature [K]
T_w	wall temperature [K]
T_∞	free stream temperature [K]
$\bar{\nabla}T$	temperature gradient [$K m^{-1}$]
u	gas velocity (z-component) [$m s^{-1}$]



- u^* friction velocity $u^* = u_m \sqrt{\frac{f}{2}}$ [m s⁻¹]
- u_m average gas velocity [m s⁻¹]
- v gas velocity (r-component) [m s⁻¹]
- V_d particle deposition velocity [m s⁻¹]
- \bar{V}_{th} thermophoretic velocity [m s⁻¹]
- z axial coordinate [-]
- z_+ dimensionless axial coordinate $z/(r_0 Re Pr)$ [-]
- z_{dep} thermal entrance length [m]
- Z dimensionless distance from the entry $Z = z/(0.05 D_t Pe_g)$ [-]

Greek letters

- α thermal diffusivity $k_g/(\rho \cdot C_p)$ [m² s⁻¹]
- β_1 thermophoretic parameter (in laminar tube flow) $\beta_1 = Pr K_{th}/(T_e - T_w)/T_w$ [-]
- δ_{df} dust free layer [m]
- ϵ_0 the permittivity of air [C² N⁻¹ m⁻²]
- η thermophoretic deposition efficiency [-]
- η_e electrostatic deposition efficiency [-]
- η_ℓ isothermal particle deposition efficiency in laminar tube flow [-]
- η_{em} thermophoretic deposition efficiency in laminar tube flow [-]
- η_t isothermal particle deposition efficiency in turbulent tube flow [-]
- η_{tur} thermophoretic deposition efficiency in turbulent tube flow [-]
- λ mean free path of air [m]
- μ air dynamic viscosity [N s m⁻²]
- μ' dimensionless deposition parameter [-]

- ν air kinematic viscosity [N s m^{-2}]
- θ dimensionless temperature difference [-]
- θ^* dimensionless temperature $T_w/(T_e-T_w)$ [-]
- ρ_g gas density [kg m^{-3}]
- ρ_p particle density [kg m^{-3}]
- τ particle relation time $\tau = \rho_p d_p^2 C / 18 \mu'$ [s]
- τ^+ dimensionless particle relation time $\tau^+ = u^{*2} / \nu$ [-]



CHAPTER 1

INTRODUCTION

Thermophoresis is a physical phenomenon that aerosol particles move toward the direction of decreasing temperature when subjected to a thermal gradient. Knowledge of thermophoresis is of great interest as it has various industrial applications. Extensive experimental and theoretical works have been published on thermophoretic coefficient (Waldmann, 1961; Brock, 1962; Derjaguin et al., 1976; Talbot et al., 1980), thermophoretic particle deposition efficiency in laminar duct and channel flow (Walker et al., 1979; Stratmann et al., 1994; Tsai and Lu, 1995), thermophoretic particle deposition efficiency in turbulent duct and channel flow (Nishio et al., 1974; Romay et al., 1998; He and Ahmadi, 1998). In industrial applications, thermophoretic force has been used to enhance particle deposition efficiency on impactor substrate (Lee and Kim, 2002); to suppress particles deposition on wafer surface (Stratmann and Fissan, 1988); to design a particle control device for diesel engine exhaust (Messerer et al., 2003).

In this chapter, literature related to thermophoretic coefficient and thermophoretic velocity, thermophoretic deposition in laminar and turbulent tube flow, isothermal deposition mechanisms in tube flow and the application of thermophoretic force to suppress particle deposition is reviewed first. The motivation of this study is also explained, followed by the objectives of this study.

1.1 Thermophoretic coefficient and thermophoretic velocity

Many previous investigators have studied the phenomena of thermophoresis

(Brock, 1962; Derjaguin et al., 1976; Talbot et al., 1980). The thermophoretic velocity can be calculated as

$$\vec{V}_{th} = -\frac{\nu K_{th}}{T} \vec{\nabla} T \quad (1.1)$$

where K_{th} is the thermophoretic coefficient derived by Derjaguin et al. (1976) as


$$K_{th} = 2.2\nu \left(\frac{k_g / k_p + C_t (2\lambda / d_p)}{1 + 2(k_g / k_p) + 2C_t (2\lambda / d_p)} \right) \quad (1.2)$$

The experimental results of Derjaguin et al. (1976) show good agreement with their own theory, but deviate from those of Talbot et al. (1980) who derived the expression for thermophoretic coefficient as

$$K_{th} = \frac{2\nu C_s C}{(1 + 3C_m (2\lambda / d_p))} \times \left(\frac{k_g / k_p + C_t (2\lambda / d_p)}{1 + 2(k_g / k_p) + 2C_t (2\lambda / d_p)} \right) \quad (1.3)$$

This formula approaches the Waldmann's free molecular formula (1961) when $Kn \gg 1$ and the continuum-regime theory of Brock (1962) when $Kn \leq 0.2$. Talbot et al. (1980) had given evidence that their expression is accurate for all regimes from free molecular to continuum flow. The thermophoretic coefficient of Talbot et al. (1980) is most widely used to calculate thermophoretic deposition efficiency in duct and channel flow, such as in Batchelor and Shen (1985), Ye et al. (1991a), Montassier et al. (1991), Stratmann et al. (1994) and He and Ahmadi (1998).

Chang et al. (1995) has investigated thermophoretic deposition in an annular flow with fixed thermal gradients between two cylinders experimentally and numerically. The implicit finite difference method was applied to solve particle transport equation due to convection, diffusion and thermophoresis when assuming fully developed flow. They found that the experimental thermophoretic deposition efficiency is generally closer to the numerical prediction using the thermophoretic coefficient of Derjaguin et al. (1976), as compared to that using thermophoretic coefficient of Talbot et al. (1980). However, the difference between the predicted deposition efficiencies obtained from the two models is too small in comparison with the magnitude of fluctuation in the aerosol source. As a result, Chang et al. (1995) stated that it is impossible to conclude which theory is more accurate.



Tsai and Lu (1995) designed a plate-to-plate thermal precipitator using forced convection heat transfer arrangement to enhance thermophoretic particle collection efficiency. They found that the thermophoretic coefficient proposed by Talbot et al. (1980) fits very well with their experimental data.

1.2 Thermophoretic deposition efficiency in laminar tube flow

Previous theories on thermophoretic deposition efficiency in laminar tube flow, listed in Table 1.1, are restricted to fully developed flow only. These equations are applicable for a long tube where gas temperature approaches that of the wall. In previous theories, Walker et al. (1979) and Batchelor and Shen (1985) considered particle transport due to convection and thermophoresis only, thermal diffusivity of particle was neglected. Such assumption is valid only when the dimensionless

deposition parameter for laminar diffusion, ε ($\varepsilon = D L/Q$), is much less than 0.0001 (Hinds, 1999). Walker et al. (1979) developed two models, one for a short tube, and another for a sufficiently long tube where gas temperature approaches that of the tube wall. For the short tube, Walker et al. (1979) solved the particle transport equation analytically and developed the following equation for thermophoretic deposition efficiency:

$$\eta = 4.07 \frac{\text{Pr} K_{th}}{\theta^*} \left(\frac{z}{Pe_g} \right)^{2/3} \phi_0 \quad (1.4)$$

Table 1.2 shows the values of dimensionless particle concentration at wall, ϕ_0 , obtained in the work of Walker et al. (1979). The values of ϕ_0 are calculated from the following equations:

$$\phi_0 = \exp \left[- \int_0^\infty \frac{f_2(\eta_1)}{f_1(\eta_1)} d\eta_1 \right] \quad (1.5)$$

where

$$f_1 = \frac{3\eta_1^2}{\text{Pr} K_{th}} (\theta^+ + \theta^*) + \frac{d\theta^+}{d\eta_1}$$

$$f_2 = 3\eta_1^2 \frac{d\theta^+}{d\eta_1} + \frac{1}{\theta^+ + \theta^*} \left(\frac{d\theta^+}{d\eta_1} \right)^2$$

$$\theta^+ = \frac{T - T_w}{T_e - T_w}$$

$$\eta_1 = Pe_g^{1/3} (1-r) \left(\frac{2}{9z} \right)^{1/3}$$

Note that Eq. (1.4) is only applicable before gas temperature is in equilibrium with the wall. In the case of a long tube, they solved the particle transport equation by the particle trajectory method and obtain the exact solution for the thermophoretic deposition efficiency, as shown in Table 1.3. An approximate expression, as can be seen in Table 1.1, was also developed by fitting the exact solutions as a function of PrK_{th} and θ^* . The difference between the exact solution and the approximate solution increases with decreasing PrK_{th} or θ^* value, and is less than 18 %.

Batchelor and Shen (1985) also found that the deposition efficiency for the long tube is a function of PrK_{th} and θ^* . Their thermophoretic deposition efficiency agrees well with Walker et al.'s exact solution (1979) only when $PrK_{th} = 1$. However, when PrK_{th} and T_e/T_w are small, the predicted thermophoretic deposition efficiency does not agree well with that predicted by Walker et al. (1979).

Stratmann et al. (1994) utilized the SIMPLER algorithm developed by Patankar (1980) to calculate the thermophoretic deposition efficiency and developed an empirical expression for predicting the thermophoretic particle deposition efficiency as shown in Table 1.1.

From the above review, the theory of the thermophoretic deposition efficiency is obviously established for fully developed flow, the entrance flow effect on particle

Table 1.1 Theoretical expressions of thermophoretic deposition efficiency for a long tube where the temperature of hot gas has approached that of the wall.

Walker et al. (1979) (approximate solution)	$\eta = \frac{\text{Pr} K_{th}}{T_w} (T_e - T_w)$
Batchelor and Shen (1985)	$\eta = \text{Pr} K_{th} \left(\frac{T_e - T_w}{T_e} \right) \left(1 + (1 - \text{Pr} K_{th}) \left(\frac{T_e - T_w}{T_e} \right) \right)$
Stratmann et al. (1994)	$\eta = 1 - \exp \left(-0.845 \left(\frac{\text{Pr} K_{th} + 0.025}{T_w / (T_e - T_w) + 0.28} \right)^{0.932} \right)$

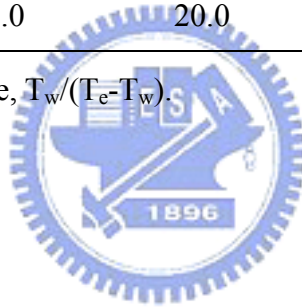
Table 1.2 The values of ϕ_0 at different $\text{Pr}K_{th}$ and θ^* for the short tube case.

$\text{Pr}K_{th}$	ϕ_0				
	$\theta^* = 1/4$	$\theta^* = 1/2$	$\theta^* = 1$	$\theta^* = 2$	$\theta^* = 4$
1.0	1/5	1/3	1/2	2/3	4/5
0.8	0.2186	0.3599	0.5314	0.6965	0.8230
0.7	0.2300	0.3760	0.5499	0.7134	0.8356
0.5	0.2599	0.4169	0.5950	0.7530	0.8642
0.3	0.3078	0.4788	0.6587	0.8048	0.8989

Table 1.3 The exact solution of Walker et al. (1979) for thermophoretic deposition efficiency in the long tube case.

PrK _{th}	thermophoretic deposition efficiency, %				
	$\theta^* = 1/4$	$\theta^* = 1/2$	$\theta^* = 1$	$\theta^* = 2$	$\theta^* = 4$
1.0	80.0	66.7	50.0	33.3	20.0
0.8	73.0	59.0	42.0	27.0	16.0
0.7	68.0	54.0	39.0	24.0	14.0
0.5	58.0	44.0	30.0	18.0	10.0
0.3	42.0	31.0	20.0	12.0	6.0

θ^* is dimensionless temperature, $T_w/(T_e - T_w)$.



deposition efficiency in tube flow has rarely been investigated. Recently, Fan et al. (1996) found that the gas collection efficiency of an annular diffusion denuder is higher for developing flow than fully developed flow. Since the highest temperature gradient and uniform velocity near the wall occur at the entrance of a tube where both flow and temperature are developing, thermophoretic deposition in the entrance region may be enhanced. Therefore, the first part of this study is to investigate the effect of developing flow in entrance region on the thermophoretic deposition efficiency under laminar flow condition.

1.3 Thermophoretic deposition efficiency in turbulent tube flow

Nishio et al. (1974) and Romay et al. (1998) derived their own expressions for the thermophoretic particle deposition efficiency in turbulent tube flow. They used the one-dimensional control volume approach for the conservation of mass shown in Fig. 1.1 and obtained the following equation:

$$\frac{dN}{N} = -\frac{\pi D_t}{Q} V_{th} dz \quad (1.6)$$

To obtain the thermophoretic velocity, the temperature gradient at the wall was calculated from the following equation:

$$k_g \left. \frac{dT}{dr} \right|_{r=r_0} = h(T_w - T_m) \quad (1.7)$$

Eq. (1.6) was then integrated along the length of the tube. Table 1.4 displays the theoretical expressions of Nishio et al. (1974) and Romay et al. (1998) are shown.

Table 1.4 Theoretical expressions of the thermophoretic deposition efficiency in turbulent tube flow.

Romay et al. (1998)

$$\eta_L = 1 - \left[\frac{T_w + (T_e - T_w) \exp(-\pi D_t h L / \rho Q C_p)}{T_{in}} \right]^{\text{Pr} K_{th}}$$

Nishio et al. (1974)

$$\eta_L = 1 - \exp \left(- \frac{\rho C_p K_{th} v (T_e - T_w)}{k_g \bar{T}} \left(1 - \exp \left(\frac{-4hL}{u_m \rho C_p D_t} \right) \right) \right)$$

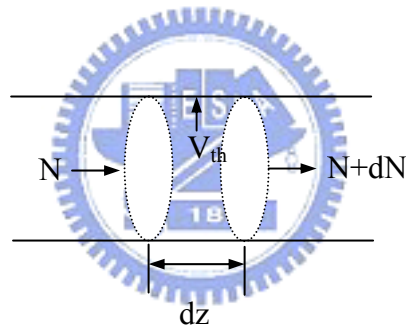


Figure 1.1 Fluid element.

Both expressions will be used later to predict the thermophoretic deposition efficiency in turbulent tube flow.

Most of the previous researches focused on the thermophoretic deposition in laminar flow regime seem to agree well with the experimental data, however, the study in turbulent tube flow by Romay et al. (1998) found that differences between their theoretical predictions and experimental data existed and increased with the flow Reynolds number. When the flow Reynolds number equaled 5517, the deviation was about 3 %, and it increases to about 10 % when the Reynolds number was increased to 9656. Similar discrepancy was found when the theoretical predictions of Romay et al. (1998) were compared with the experimental data of Nishio et al. (1974). This indicates that there must be some other mechanisms affecting the deposition especially in the turbulent flow. Romay et al. (1998) argued that the discrepancy may be due to inertially enhanced thermophoresis for laminar flow over curved surfaces (Konstandopoulos and Rosner, 1995) and enhanced thermophoresis caused by non-uniform concentration gradients and reverse thermophoresis in the preparation of heated aerosol source (Weinberg, 1982). Therefore it is worthwhile for this study to obtain more accurate particle deposition efficiency data to validate the theoretical equations of thermophoretic deposition efficiency in turbulent flow regime.

1.4 Isothermal particle deposition mechanisms in tube flow

Besides thermophoresis, there are many other particle deposition mechanisms in tube flow, such as laminar diffusion, particle electrostatic deposition, gravitational settling and turbulent diffusional and inertial deposition. The particle diffusional penetration in laminar tube flow is (Hinds, 1999):

$$P_{d,\ell} = 1 - 5.50\mu'^{2/3} + 3.77\mu', \text{ for } \mu' < 0.007 \quad (1.8)$$

$$P_{d,\ell} = 0.819 \exp(-11.5\mu') + 0.0975 \exp(-70.1\mu'), \text{ for } \mu' \geq 0.007 \quad (1.9)$$

where $\mu' = \frac{DL}{Q}$ and $D = KTB$. The particle penetration decreases with an increasing μ' . When $\mu' < 0.001$, the penetration is close to 1.0. When $\mu' > 0.3$, the penetration is close to zero and almost all particles deposit on the tube wall.

For submicron particles used in this study, gravitational settling is usually not important while laminar diffusion and electrostatic deposition can be important. Cohen et al. (1995) passed monodisperse singly charged particles through a conducting copper tube (ID= 1.9 cm) and found that particle deposition efficiencies varied from 1 to 4% for particle diameter ranged from 0.015 - 0.095 μm at a mean flow rate of 4.6 l min^{-1} under laminar flow condition. However the corresponding theoretical efficiencies by Pich (1978) were only from 0.04 to 0.11%. The electrostatic particle deposition efficiency is calculated as (Pich, 1978):

$$\eta_e = (6\tau_e)^{1/3} \quad (1.10)$$

where

$$\tau_e = \frac{q^2 t C}{4\pi\epsilon_0 F r_0^3} \quad (1.11)$$

$$F = 3\pi\mu' d_p \quad (1.12)$$

In addition, Yu and Chandra (1978) derived the following equation for calculating the

critical particle radial position, r_c , to obtain the electrostatic particle deposition efficiency as :

$$\frac{r_0}{r_c} + 2 \ln \frac{r_c}{r_0} - \left(\frac{r_c}{r_0} \right)^2 + \frac{1}{3} \left(\frac{r_c}{r_0} \right)^3 - \frac{1}{3} = \frac{Z_p K_E n_p e t}{D_t^3} \quad (1.13)$$

The critical particle radial position is defined such that all particles starting at the tube entrance with $r > r_c$ will deposit on the tube wall. After obtaining r_c , the particle deposition efficiency can be calculated as:

$$\eta_e = \left(1 - \left(\frac{r_c}{r_0} \right)^2 \right)^2 \quad (1.14)$$

Eqs. (1.10) and (1.14) are the expressions for predicting the deposition efficiency of charged particles due to image force. The deposition efficiency due to space charge is derived by Kasper (1981) as:

$$\eta_e' = 1 - \frac{1}{1 + N_e E t} \quad (1.15)$$

where $E = 4\pi B q^2$.

Ye et al. (1991b) studied the electrostatic deposition efficiency of an annular denuder and found singly charged particles and particles in Boltzmann charge equilibrium had higher deposition efficiency than neutral particles. For example, for a 0.03 μm particle the deposition efficiencies for Boltzmann charge equilibrium

condition and neutral condition are 12.6 % and 2.4 %, respectively, and for a 0.75 μm particle the deposition efficiencies are 4.0 % and 1.5 %, respectively. Some previous investigators who used particles in Boltzmann charge equilibrium as test particles could obtain inaccurate deposition efficiency data for thermophoretic deposition efficiency. That is, even for conductor tubing and for particles that are in Boltzmann charge equilibrium, the deposition efficiency due to electrostatic is still important and must be measured carefully. Therefore, in this study, particles in both Boltzmann charge equilibrium and charge neutral conditions were used and experimental data were compared to see possible influences.

When flow is turbulent, aerosol particles transport toward the inner wall of a tube is substantially enhanced because of eddy diffusion. Friedlander (2000) gave the particle deposition velocity towards the tube wall due to eddy diffusion

$$V_d = 0.0118 \text{Re}^{7/8} \text{Sc}^{1/3} (D/D_t) \quad (1.16)$$

The particle penetration efficiency can be calculated as

$$P_d = \exp(-\pi D_t V_d L / Q) \quad (1.17)$$

Eq. (1.16) indicates that small particles tend to have higher V_d hence higher deposition efficiency. This is because small particles (less than 0.1 μm) follow eddy motion easily resulting an increase in wall deposition rate. While large particles greater than 1.0 μm are unable to follow eddy motion smoothly and can be projected to the wall due to inertial force through the relatively quiescent fluid near the tube

surface. This causes deposition rate of large particles to be increased. Such mechanism is called turbulent deposition. Lee and Gieseke (1994) investigated deposition rate of aerosol particles on tube wall under turbulent flow condition. Experimental results of Lee and Gieseke (1994) show that among the existing theories, the theory proposed by Friedlander and Johnstone (1957) is found to be agreed well with their experimental data or the experimental results of Liu and Agarwal (1974) in the regimes of inertial impaction deposition mechanisms. The dimensionless particle deposition velocity of turbulent deposition, developed by Friedlander and Johnstone (1957) is

$$\begin{aligned}
 V_d^+ = V_d/u^* &= \frac{1}{1883/(\tau^+)^2 - 50.6 + 1/\sqrt{f/2}}, \text{ for } 0.9\tau^+ \leq 5 \\
 &= \frac{1}{5 \ln \frac{5.04}{0.9\tau^+ / 5 - 0.96} - 13.73 + 1/\sqrt{f/2}}, \text{ for } 5 < 0.9\tau^+ \leq 30 \\
 &= \sqrt{f/2}, \text{ for } 0.9\tau^+ < 5
 \end{aligned} \tag{1.18}$$

The penetration efficiency is computed using Eq. (1.17).

After reviewing the previous studies, it was found that there still exist some unclear points on the thermophoretic particle deposition efficiency in tube flow. As a result, thermophoretic particle deposition on tube wall under laminar and turbulent flow conditions will be investigated experimentally in this study. The particular geometry of interest was flow through a cylindrical tube where the aerosol was heated to a specified temperature and then cooled by abruptly decreasing the wall temperature to a constant value, and thus a thermophoretic force on the particles was induced causing them to drift toward and deposit onto tube wall. In the experiment,

isothermal deposition mechanisms were also measured first by setting the wall temperature the same as gas flow. In the actual thermophoretic deposition experiment, deposition efficiencies due to isothermal deposition mechanisms can then be assessed and the deposition efficiency due to thermophoresis alone can be obtained accurately.

1.5 Application of thermophoretic force to suppress particle deposition

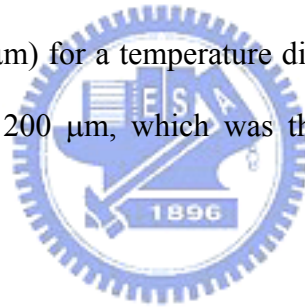
There are studies on preventing particle deposition on wafer surface. In contrast there is no literature concerning the suppression of particle deposition in a tube flow. In practical application, such as in the semiconductor industry, a common practice is to heat up the tube wall to prevent particle deposition. However, the required wall temperature to effectively suppress particle deposition in the tube is unknown. The last part of this study further conducts numerical analysis to quantify particle deposition efficiency using different tube wall temperatures that are higher than the inlet gas flow under laminar tube flow condition. The numerical results will then be verified with the experimental data. The numerical results will also be used to develop an empirical expression for predicting the minimum wall temperature needed to effectively suppress diffusional particle deposition by thermophoretic force.

To reduce particle deposition on wafer surface, thermophoretic force is usually used, e.g., by Stratmann et al. (1988), Ye et al. (1991a) and Bae et al. (1995). Stratmann et al. (1988) derived an expression for the thickness of the dust-free layer for flow over a free-standing wafer. As the temperature gradient at the wall and the velocity component normal to the wall were known, the particle equation of motion obtained from the equilibrium of inertial force, drag force and thermophoretic force

on the particle was solved to find the thickness of the dust-free layer near the forward stagnation point of the wafer surface. According to Stratmann et al. (1988), the analytical expression of the dust free layer thickness is,

$$\delta_{df} = 0.961 \left(\frac{v}{a} \right)^{1/2} K_{th}^{1/2} \left[\frac{T_w - T_\infty}{T_w} \right]^{1/2} Pr^{0.189} \quad (1.19)$$

The above equation states that the dust-free layer thickness depends on the temperature difference between the gas flow and wafer surface. However, there is no analytical solution available yet for thermophoretic particle deposition velocity at an arbitrary temperature difference. Based on Eq. (1.19), δ_{df} for aluminum and copper particles ($0.5 < d_p < 2 \mu\text{m}$) for a temperature differences as small as $10 \text{ }^\circ\text{C}$ was found to range from 100 to 200 μm , which was thick enough to prevent particle deposition.



Ye et al. (1991a) used the SIMPER algorithm to solve the coupled Navier-Stokes, energy and convection-diffusion equations to obtain the velocity, temperature and concentration fields. The convection-diffusion equation took into account the external forces of sedimentation and thermophoresis. The measured particle deposition velocity on the wafer surface was found to decrease with an increasing temperature of the surface, and agree with the numerical results. It was shown that by heating the wafer surface to a temperature $10 \text{ }^\circ\text{C}$ higher than the air flow, a clean zone between 0.03 to $1.0 \mu\text{m}$ particles was created. The experimental study of Bae et al. (1995) also showed that by raising the wafer surface temperature by $5 \text{ }^\circ\text{C}$ higher than the surrounding air, the average deposition particle velocity in the range from 0.1 to $1 \mu\text{m}$ in diameter was reduced to less than 10^{-4} cm/s .

1.6 Objectives of this study

The objectives of this study are summarized as:

1. To investigate the effect of developing flow at entrance region on thermophoretic particle deposition efficiency numerically.
2. To investigate the effect of particle electrostatic charge on thermophoretic particle deposition efficiency in tube flow under laminar and turbulent flow conditions experimentally.
3. To conduct numerical analysis and experiments to study thermophoretic effect on particle deposition efficiency in laminar tube flow.



CHAPTER 2

NUMERICAL METHODS

In section 2.1, the temperature fields obtained either from the analytical solution or numerical simulation are discussed. Then the critical trajectory method for calculating the thermophoretic particle deposition efficiency is presented. In the last section of this chapter, the method used to solve convection-diffusion equation to obtain particle deposition efficiency when the temperature of tube wall is higher than gas flow is described.

2.1 Temperature field

In laminar flow, the entry length for the velocity profile to become fully developed given by Incropera and De Witt (1996) is

$$\left(\frac{z}{D_t}\right)_{dep} \cong 0.05 \text{ Re} \quad (2.1)$$

and the entry length for the temperature profile to become fully developed is (Kays and Crawford, 1980)

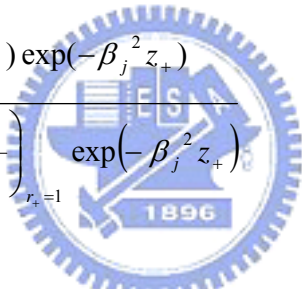
$$\left(\frac{z}{D_t}\right)_{dep} \cong 0.05 \text{ Re Pr} = 0.05 \text{ Pe}_g \quad (2.2)$$

That is, temperature is fully developed earlier than velocity when $\text{Pr} < 1$. In case that thermal entrance length is much shorter than the total tube length, one can

assume that temperature is fully developed.

Fully developed flow and temperature fields

The case of the fully developed flow and temperature fields is discussed first. When temperature is fully developed, the dimensionless temperature profile $(T_w - T)/(T_w - T_m)$ is invariant in the axial direction, and is a function of radial coordinate only. When the dimensionless distance Z is greater than the dimensionless thermal entry length, the invariant temperature profile can be expressed as (Skelland, 1974).

$$\frac{T_w - T}{T_w - T_m} = \frac{\sum_{j=1}^{j=\infty} B_j \phi_j(r_+) \exp(-\beta_j^2 z_+)}{\sum_{j=1}^{j=\infty} \frac{-4B_j}{\beta_j^2} \left(\frac{d\phi_j}{dr_+} \right)_{r_+=1} \exp(-\beta_j^2 z_+)} \quad (2.3)$$


where

$$r_+ = \frac{r}{r_0}, \quad z_+ = \frac{z/r_0}{\text{Re Pr}}$$

$$\phi_j(r_+) = \sum_{i=0}^{i=\infty} \alpha_{ji} r_+^i, \quad \alpha_{ji} = 0 \quad \text{for } i < 0$$

$$\alpha_{ji} = 1 \quad \text{for } i = 0, \quad \alpha_{ji} = -\beta_j^2 (\alpha_{i-2} - \alpha_{i-4}) / i^2$$

$$\beta_j = 4(j-1) + \frac{8}{3}; \quad j=1,2,3,\dots$$

$$B_j = (-1)^{j-1} \times 2.84606 \beta_j^{-\frac{2}{3}}$$

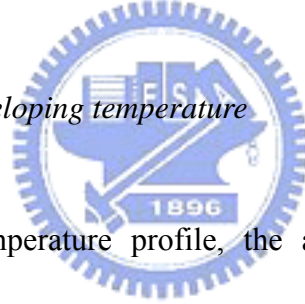
$$\frac{-B_j}{2} \left(\frac{d\phi_j}{dr_+} \right)_{r_+=1} = 1.01276 \beta_j^{-\frac{1}{3}}$$

The polynomial function obtained from curve fitting the calculated temperature profile from Eq. (2.3) is

$$\frac{T_w - T}{T_w - T_m} = 1.734 \left(\frac{r}{r_o} \right)^3 - 3.487 \left(\frac{r}{r_o} \right)^2 - 0.041 \left(\frac{r}{r_o} \right) + 1.805 \quad (2.4)$$

Eq. (2.4) is then used to obtain the temperature gradient, and the corresponding thermophoretic velocity for this case.

Fully developed flow and developing temperature



For the developing temperature profile, the analytical solution of Graetz's problem is (Skelland, 1974)

$$\frac{T_w - T}{T_w - T_e} = \sum_{j=1}^{j=\infty} B_j \phi_j(r_+) \exp(-\beta_j^2 z_+) \quad (2.5)$$

The dimensionless developing temperature profiles of Eq. (2.5) are compared with that described in Grigull and Traz (1965) and found both profiles agree very well, as indicated in Fig. 2.1.

Developing flow and temperature

In order to calculate developing temperature field, the following

two-dimensional developing velocity field derived by Sparrow et al. (1964) was used:

$$\frac{u}{u_m} = \omega = 2(1 - R^2) + \sum_{i=1}^{\infty} \frac{4}{\sigma_i^2} \left[\frac{J_0(\sigma_i R)}{J_0(\sigma_i)} - 1 \right] e^{-\sigma_i^2 Z^*} \quad (2.6)$$

where

$$\sigma_1 = 5.13562, \quad \sigma_{i+1} = \sigma_i + \pi, \quad i = 1, 2, 3, \dots$$

$$Z^* = \frac{z^* v}{u_m r_0^2}$$

$$z = \int_0^{z^*} \varepsilon dz^*$$

$$\varepsilon = \frac{\int_0^1 (2\omega - 1.5\omega^2)(\partial\omega/\partial X^*) R dR}{(\partial\omega/\partial R)_1 + \int_0^1 (\partial\omega/\partial R)^2 R dR}$$

Fig. 2.2 exhibits the developing velocity profiles calculated from Eq. (2.6). Eq. (2.6) was then used to calculate the developing temperature field for developing flow numerically by solving the following 2-D cylindrical energy equation:

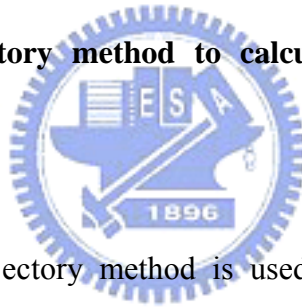
$$u \frac{\partial T}{\partial z} + v \frac{\partial T}{\partial r} = \alpha \left(\frac{1}{r} \frac{\partial T}{\partial r} + \frac{\partial^2 T}{\partial r^2} \right) \quad (2.7)$$

where the boundary conditions are

$$T(r, 0) = T_e; \quad T(r_0, z) = T_w; \quad \frac{\partial T}{\partial r}(0, z) = 0$$

In the numerical simulation for developing temperature field, the finite volume method and SIMPLE algorithm (Patankar, 1980) were used. In the test run, the number of grid in the computational domain was either 4,000 (100 in the axial direction \times 40 in radial direction), 12,000 (200 in the axial direction \times 60 in radial direction) or 24,000 (300 in the axial direction \times 80 in radial direction). The numerical results indicate that the number of grid of 12,000 is accurate enough and was adopted in the further study. The cell spacing is finer near the wall and inlet where temperature gradients in radial direction are expected to be larger. In the simulation, the influence of radial fluid velocity and temperature-dependent fluid properties on thermophoretic deposition efficiency was accounted for.

2.2 Critical particle trajectory method to calculate thermophoretic particle deposition efficiency



The critical particle trajectory method is used to obtain the thermophoretic particle deposition efficiency when neglecting particle diffusion. The critical particle trajectory is shown in Fig. 2.3. A particle starts at the critical radial position, r_c , at the entrance will deposit just at the end of the tube of length L . The annular-hatched region from r_c to r_0 is the particle deposition region where a particle starts will deposit somewhere on the wall of the tube. When flow is fully developed, analytical temperature field is available and the particle equations of motion can be solved to obtain the critical radial position and the thermophoretic deposition efficiency. However, when both flow and temperature are developing (or combined developing case), there is no analytical equation for temperature field. In this study, it is found that developing velocity field simulated numerically by finite difference

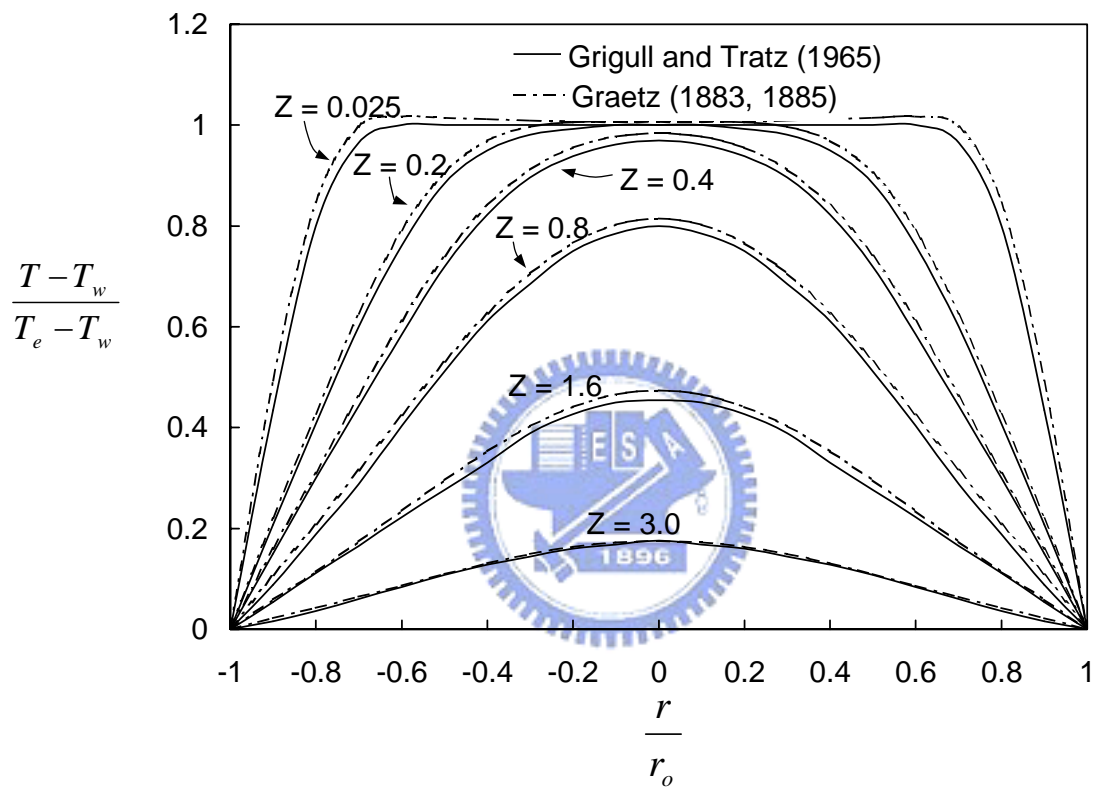


Figure 2.1 Comparison between Graetz's solution and temperature profile in the thermal entry region with that of Grigull and Tratz (1965).

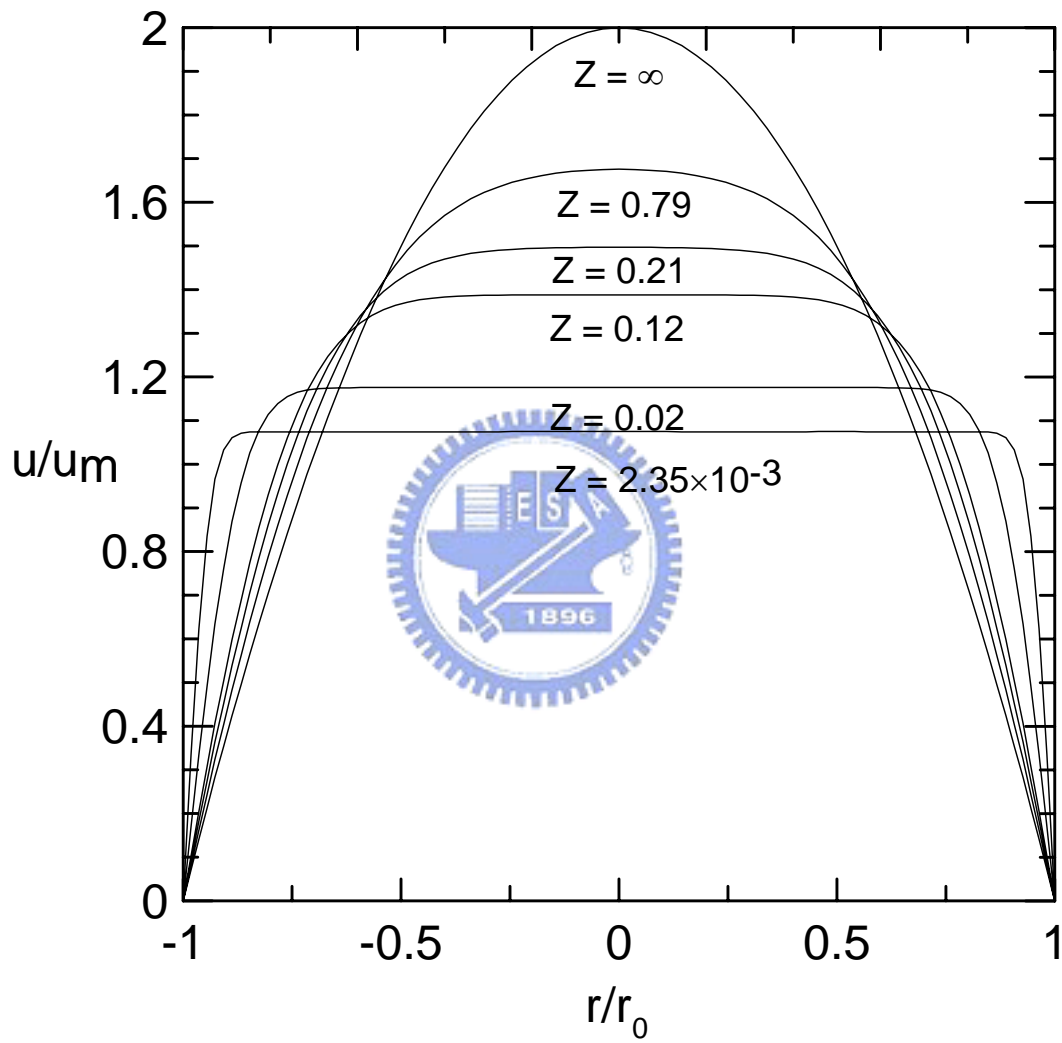


Figure 2.2 The developing velocity profiles in laminar tube flow.

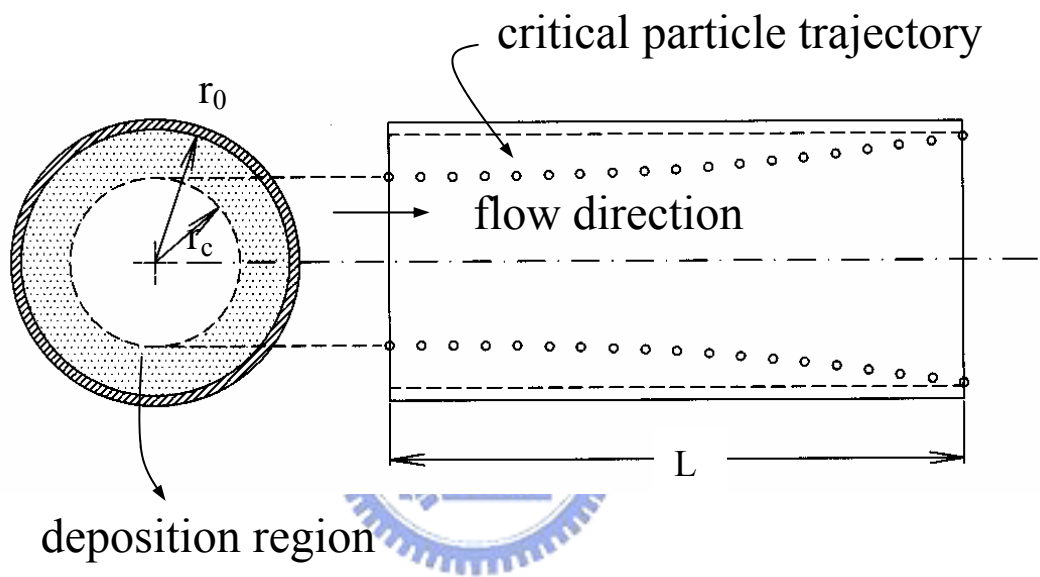


Figure 2.3 Critical particle trajectory.

method is not accurate. Therefore, the analytical velocity distribution developed by Sparrow et al. (1964) was used to calculate the developing temperature profile numerically, and then the critical particle trajectory and deposition efficiency was obtained by solving the particle equations of motion.

In the cylindrical coordinate, the particle equations of motion in the z (radial) and r (axial) directions are respectively

$$\frac{d^2 z}{dt^2} = C_d \frac{Re_p}{24} \frac{(u - dz/dt)}{\tau} \quad (2.8)$$

and

$$\frac{d^2 r}{dt^2} = C_d \frac{Re_p}{24} \frac{(v - dr/dt)}{\tau} + \frac{V_{th}}{Bm_p} \quad (2.9)$$

where C_d is the drag coefficient proposed by Rader and Marple (1985),

$$C_d = \frac{24}{Re_p} (1 + 0.0916 Re_p), \quad Re_p < 5 \quad (2.10)$$

and

$$C_d = \frac{24}{Re_p} (1 + 0.158 Re_p^{2/3}), \quad 5 < Re_p < 1000 \quad (2.11)$$

To calculate the values of B and τ in Eq. (2.9), the C value, slip correction factor, should be calculated first. A fitted expression of C values to air data for particles is given by Allen and Rabbe (1985) as

$$C = 1 + Kn[a + b \exp(-c / Kn)] \quad (2.12)$$

For solid particles, $a=1.142$, $b=0.558$ and $c=0.999$ (Allen and Rabbe, 1985) while for oil droplets, $a=1.207$, $b=0.440$ and $c=0.596$ (Rader, 1990). It is noted that the deviation of C values between these two materials is very small, which is less than 4.1 % for particle sizes in the range of 0.001 to 1 μm at temperature of 293 K and pressure of 1 atm. Therefore, we decide to use the equation provided by Allen and Rabbe (1985) to calculate the C value.

In order to calculate thermophoretic deposition efficiency, the critical radial position of particle trajectory, r_c , should be known. For the combined fully developed case, the analytical equation listed in the appendix A, Eq. (A.6), is solved to obtain r_c and the corresponding efficiency. For fully developed flow and developing temperature case, the particle equations of motion have to be solved numerically by the fourth order Runge-Kutta method. For the combined developing case, the particle equations of motion of Eqs. (2.8) and (2.9) were integrated numerically by means of the fourth order Runge-Kutta method. As the particle equations of motion are integrated through the domain of interest, initial velocity is given equal to the average gas flow velocity, and the initial position is set at the entrance of the tube. The new particle position and velocity after a small increment of time is calculated by numerical integration. The procedure is repeated until the particle hits the tube wall or leaves the calculation domain.

After obtaining the critical radial position, r_c , the efficiency of thermophoretic deposition for fully developed flow is calculated in the following equation assuming the particle concentration is uniform at the inlet,

$$\eta_f = \frac{\int_{r_c}^{r_0} 2u_m \left(1 - \frac{r^2}{r_0^2}\right) 2\pi r dr}{u_m \pi r_0^2} = 1 - 2\left(\frac{r_c}{r_0}\right)^2 + \left(\frac{r_c}{r_0}\right)^4 \quad (2.13)$$

For the combined developing case, besides assuming uniform particle concentration, the velocity profile is known to be uniform at the entrance of the tube, and the deposition efficiency can be calculated as

$$\eta_d = 1 - \left(\frac{r_c}{r_0}\right)^2 \quad (2.14)$$

2.3 Solutions of convection-diffusion equation to obtain thermophoretic particle deposition efficiency

For predicting particle deposition efficiency in a circular tube, the fully developed flow field was used. The temperature field was obtained numerically from energy equation, Eq. (2.7), by controlling the temperature of tube wall either higher or lower than gas flow.

Particle concentration field was obtained numerically by solving the following particle convection-diffusion equation:

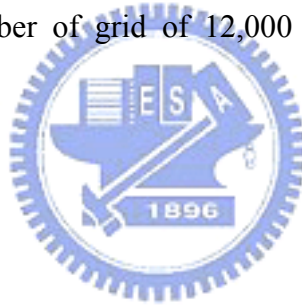
$$\nabla \cdot (\bar{u}N) = \nabla \cdot (D\nabla N) - \nabla \cdot (\vec{V}_{th}N) \quad (2.15)$$

with the following boundary conditions:

$$N(r,0) = N_e ; N(r_0, z) = 0 ; \frac{\partial N}{\partial r}(0, z) = 0 \quad (2.16)$$

In Eq. (2.15) the thermophoretic coefficient K_{th} , Eq. (1.3), proposed by Talbot et al. (1980) was used to calculate thermophoretic velocity, \vec{V}_{th} .

The particle convection-diffusion equation was also solved by the finite volume method using SIMPLE algorithm (Patankar, 1980). In the test run, three different numbers of grids in the computational domain: 4,000 (100 in the axial direction \times 40 in radial direction), 12,000 (200 in the axial direction \times 60 in radial direction) or 25,200 (280 in the axial direction \times 90 in radial direction) were used. The numerical results showed that the number of grid of 12,000 was accurate enough and was adopted in the further study.



CHAPTER 3

EXPERIMENTAL METHODS

The experimental setup for particle deposition experiment is shown in Fig. 3.1 while that for suppression experiment is illustrated in Fig. 3.2. The experimental system consists of three parts: (1) the aerosol generation and conditioning section, which produces monodisperse aerosol with known diameter with a predetermined temperature; (2) the experimental section, which establishes a temperature gradient between the tube wall and gas to induce or suppress particle deposition on tube wall by thermophoresis; and (3) temperature, flow and particle measurement systems, which measure the particle deposition efficiency at a certain flow rate and temperature gradient.



3.1 Aerosol generation and conditioning

The aerosol was generated by a Collison atomizer and mixed with clean dry air in a mixing tank, and then passed through a silica gel diffusion dryer. After drying, the aerosol was neutralized by a TSI 3077 electrostatic charge neutralizer. After neutralization, the aerosol was passed through a differential mobility analyzer (DMA; TSI 3081 Long DMA column) where a high-voltage was applied to select particles of a known electrical mobility. The monodisperse aerosol from the DMA was neutralized again and mixed with clean dilution air in another mixing tank to conduct experiment for particles in Boltzmann charge equilibrium. For the experiment involving only completely charge neutral (or zero charge) particles, an electrical condenser was used between the neutralizer and mixing tank to remove all charged particles.

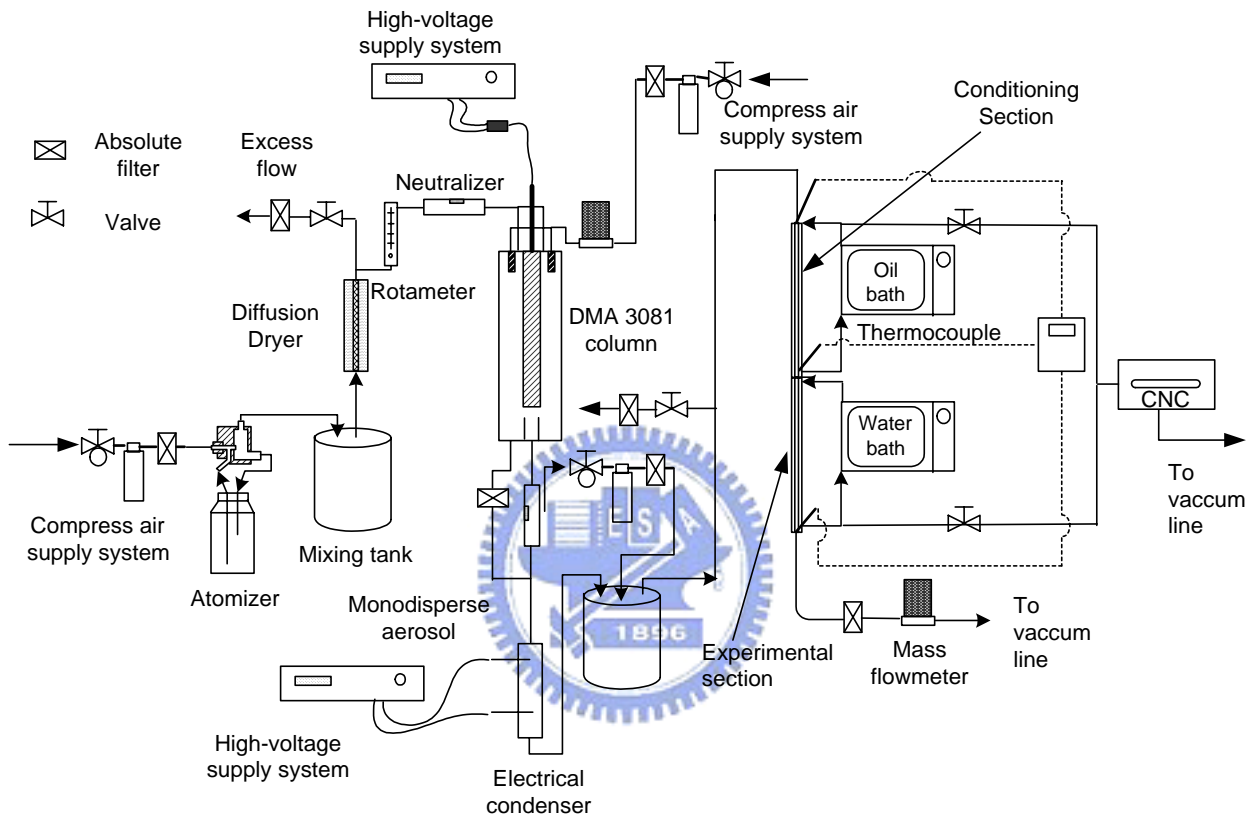


Figure 3.1 The schematic diagram of the experimental setup for deposition experiment.

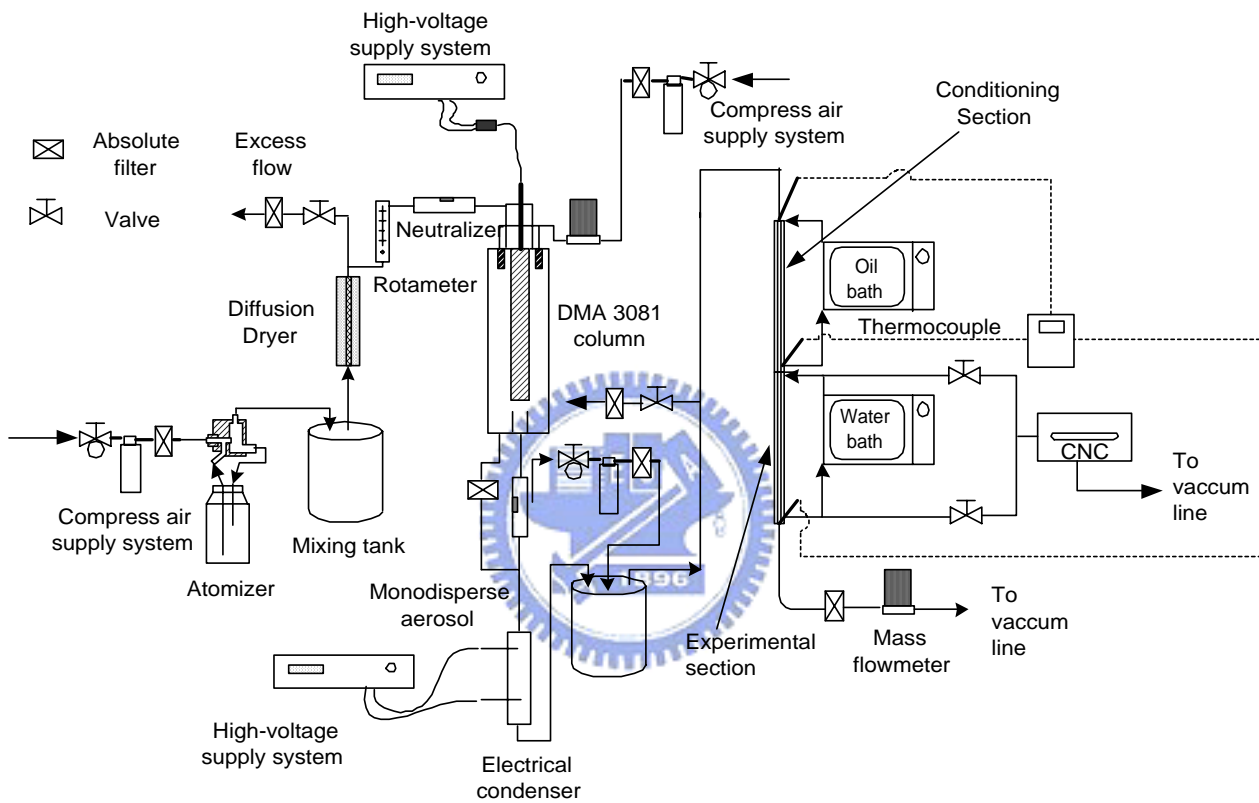
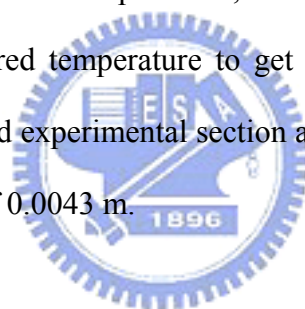


Figure 3.2 The schematic diagram of the experimental setup for suppression experiment.

3.2 Experimental system

The experimental system was further divided into two parts: (1) the conditioning section: the monodisperse aerosol stream was passed through the conditioning section, which was heated to a desired temperature by a heat exchanger for deposition experiment (i.e. thermostated silicon-oil bath). However, for suppression experiment, the temperature of conditioning section was kept constant (296 K), (2) the experimental section: for deposition experiment, the tube wall temperature was kept at 296 K by another heat exchanger (thermostated water bath) to establish a temperature gradient between the gas and wall of the tube in order to induce deposition by thermophoresis. For suppression experiment, the tube wall-temperature of this section was heated to a desired temperature to get the zero deposition. The tube lengths of the conditioning and experimental section are 1.56 and 1.18 m, respectively, with an inner tube diameter of 0.0043 m.



Three thermocouples—at the inlet of conditioning section, at the outlet of the experimental section, and at the junction between the conditioning section and experimental section—were installed to monitor the temperature at these points of the aerosol stream. The aerosol coming out from the experimental section was passed through a filter and then mass flow-controlling device (MKS Instruments, Inc.) before it was exhausted into a vacuum line. The aerosol concentrations at the inlet and at the outlet of the experimental section was measured using TSI-3760 cleanroom condensation nucleus counter (CPC), which had a sample flow rate of 1.5 l min^{-1} .

For the deposition experiment, the particle material used was NaCl. Normally 0.5 % w/v aqueous solution of NaCl was usually used. The concentration was

increased to about 1.5 % for the larger particle sizes ($d_p > 0.35 \mu\text{m}$) investigated. While for the suppression measurement, the particles used were NaCl or oleic acid generating from 1.0 % w/v aqueous NaCl solution or 2 %, v/v oleic acid dissolved in alcohol. Mass flow controller, rotameter and CPC were calibrated prior to experimental studies. Particle size distributions for the material used, were carried out to check the DMA performance. Leak test was performed some time in between the experiments to prevent the particle loss by leaking and the particle contamination from ambient air (however the experiment was carried out at ambient pressure). The flow rate of sheath air and polydisperse aerosol stream to DMA was kept constant, i.e. 5 and 0.5 l min^{-1} , respectively, through out the study.

3.3 Experimental procedure



Aerosol material solution was taken in atomizer and then turned on the atomizer. The applied voltage in voltage-supplier was adjusted to get the particle of desired size from DMA. The experimental section flow rate was then set using the downstream mass flow controller and the dilution air flow valve. For the deposition studies, the gas temperature at the conditioning section was heated to a desired value using the heat exchanger, while the temperature of the experimental section was kept constant (296 K) throughout this study. After stabilizing the conditions of the system, the particle concentrations at the inlet of the conditioning section and the outlet of experimental section were measured to determine the total deposition efficiency by CPC using operating the inlet and outlet valve. After deducting deposition efficiencies due to other particle deposition mechanisms from the total deposition efficiencies, the experimental thermophoretic deposition efficiency can be obtained. During the measurement process, it was found that the isothermal deposition in the

conditioning section could be suppressed completely when the tube wall temperature was heated higher than 343 K, which was the minimum temperature in the conditioning section. Therefore, it is not necessary to consider particle deposition losses in this section.

Whereas, for suppression studies, the temperature of conditioning section was kept constant (296 K), and the temperature of experimental section was heated to the desired temperature from 296 to 315 K by heat exchanger with a thermostated water bath to establish a temperature difference between the gas and the tube wall for the particle deposition suppression experiment. The particle deposition efficiency at a certain flow rate and particle diameter was determined from the particle number concentration data at the inlet and outlet of the experimental section. The deposition efficiency due to pure laminar flow convection diffusion was first obtained when the tube wall and aerosol stream were both kept at the temperature of 296 K. Then the tube wall temperature was raised to a desired temperature for determining the reduced deposition efficiency due to thermophoresis. The test was repeated for different flow rates and particle sizes.

The above procedure was repeated for different flow rates and particle sizes. For one data at particular test condition, average deposition from 6-8 data sets was taken, where each set contained 10 readings of the inlet, and of the outlet. The measurement time was 1-2 min/10 readings excluding system stabilization time, which was varied anywhere from 20-100 sec/reading. After completion of one data set reading, the experimental section was cleaned by passing clean air through it. The experimental conditions tested are given in Table 3.1 for deposition experiment and Table 3.2 for suppression experiment.

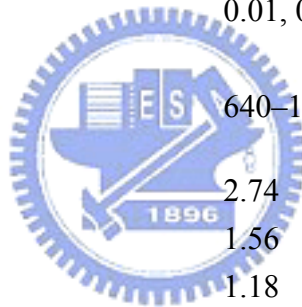
Table 3.1 Experimental conditions of deposition measurement.

Parameter	Condition
Pressure inside the tube	1 atm
Inside flow rate, l min ⁻¹	4, 20 and 32
Inlet temperature, K	
Conditioning section	296-398
Experimental section	296
Voltage on the inner collector rod, volts	75 – 4800
Particle size, μm	0.038-0.498 ^a
Reynolds numbers	1340–10200
Tube length, m	2.74
Conditioning section	1.56
Experimental section	1.18
Tube inner diameter, cm	0.43
Particle material	NaCl

^a There are 18 particle sizes in the deposition experiment. They are 0.038, 0.054, 0.08, 0.1, 0.118, 0.136, 0.152, 0.17, 0.19, 0.214, 0.26, 0.294, 0.33, 0.364, 0.397, 0.431, 0.464 and 0.498 μm in diameter.

Table 3.2 Experimental conditions of suppression measurement.

Parameter	Condition
Pressure inside the tube	1 atm
Inside flow rate, l min ⁻¹	2, 3 and 5
Inlet temperature, K	
Conditioning section	296
Experimental section	296-315
Voltage on the inner collector rod, volts	6 – 83
Particle size, μm	0.01, 0.02 and 0.04
Reynolds numbers	640–1600
Tube length, m	
Conditioning section	2.74
Experimental section	1.56
Experimental section	1.18
Tube inner diameter, cm	0.43
Particle material	NaCl or oleic acid



CHAPTER 4

ENTRANCE EFFECT ON THE THERMOPHORETIC DEPOSITION EFFICIENCY

4.1 Thermophoretic deposition efficiency for fully developed temperature and velocity fields

Fig. 4.1 compares the thermophoretic deposition efficiency of the present study and previous theories at a flow rate of 5 l min^{-1} for the pipe geometry described in the experiment of Romay et al. (1998). The fluid and particle properties used in the calculation were estimated at the averaged temperature of inlet gas and tube wall. The tube length is 0.905 m, tube diameter is 0.0049 m and the Reynolds number of the gas flow equals 1423 which is in the laminar flow region. The thermal conductivity is 6.0 W/(mK) for NaCl particle (Romay et al., 1998). Fig. 4.1 shows that the deposition efficiency of submicron particle agrees well with the prediction of Stratmann et al. (1994) and Batchelor and Shen (1985) for the long tube, the deviation is smaller than 2 %. It can be seen that the thermophoretic deposition efficiency increases at first with an increasing inlet gas temperature and decreasing particle size, but when particle size is further decreased to $0.05\mu\text{m}$ and $0.03\mu\text{m}$, the thermophoretic deposition efficiency remains almost the same (Fig. 4.1). In Fig. 4.2, the deposition efficiency calculated by the expression of Stratmann et al. (1994) (see Table 1.1) is compared with the present study. It shows the present theory is in very good agreement with the expression of Stratmann et al. (1994).

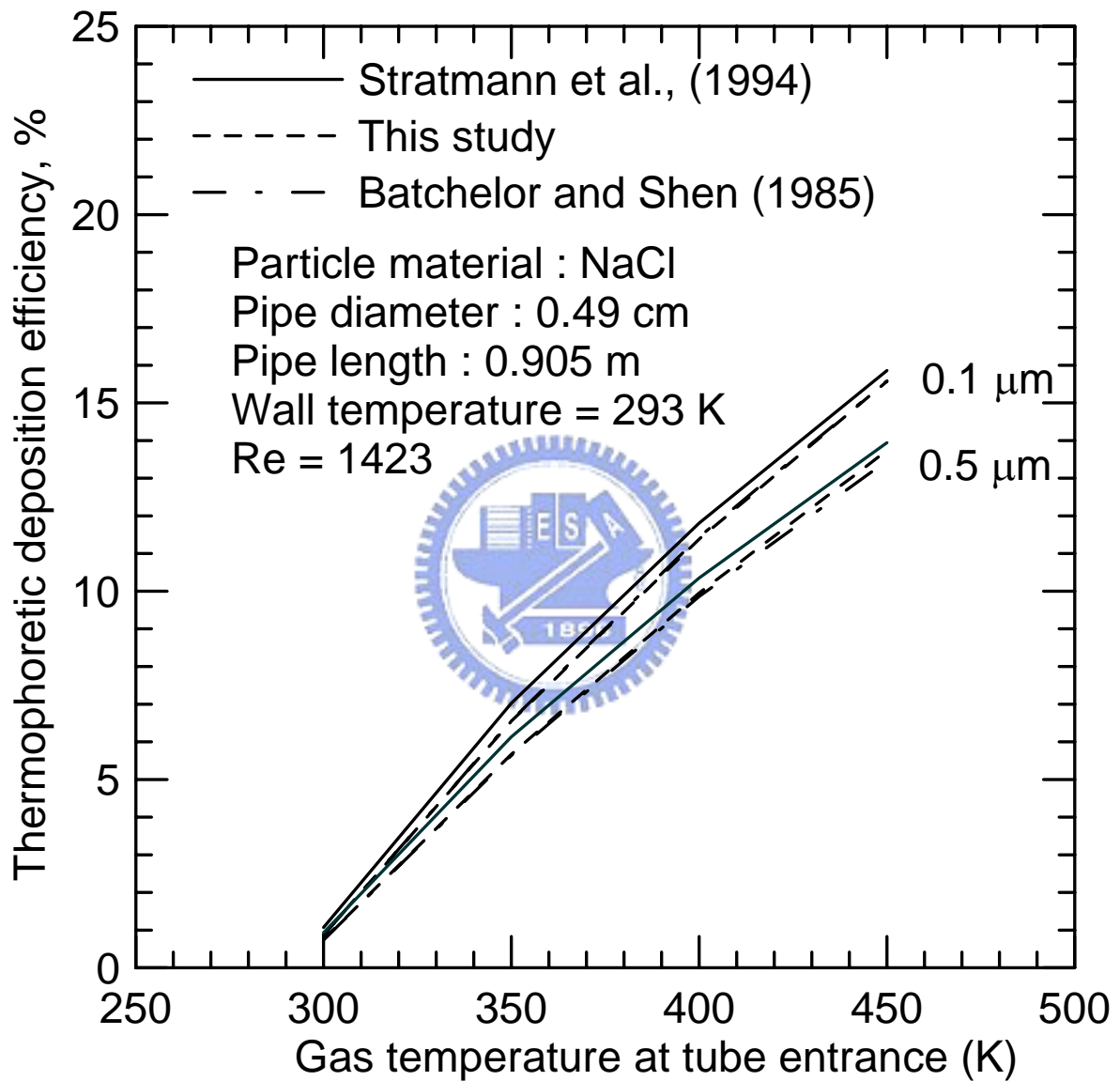


Figure 4.1 Comparison of theoretical deposition efficiency with previous theories in laminar tube flow.

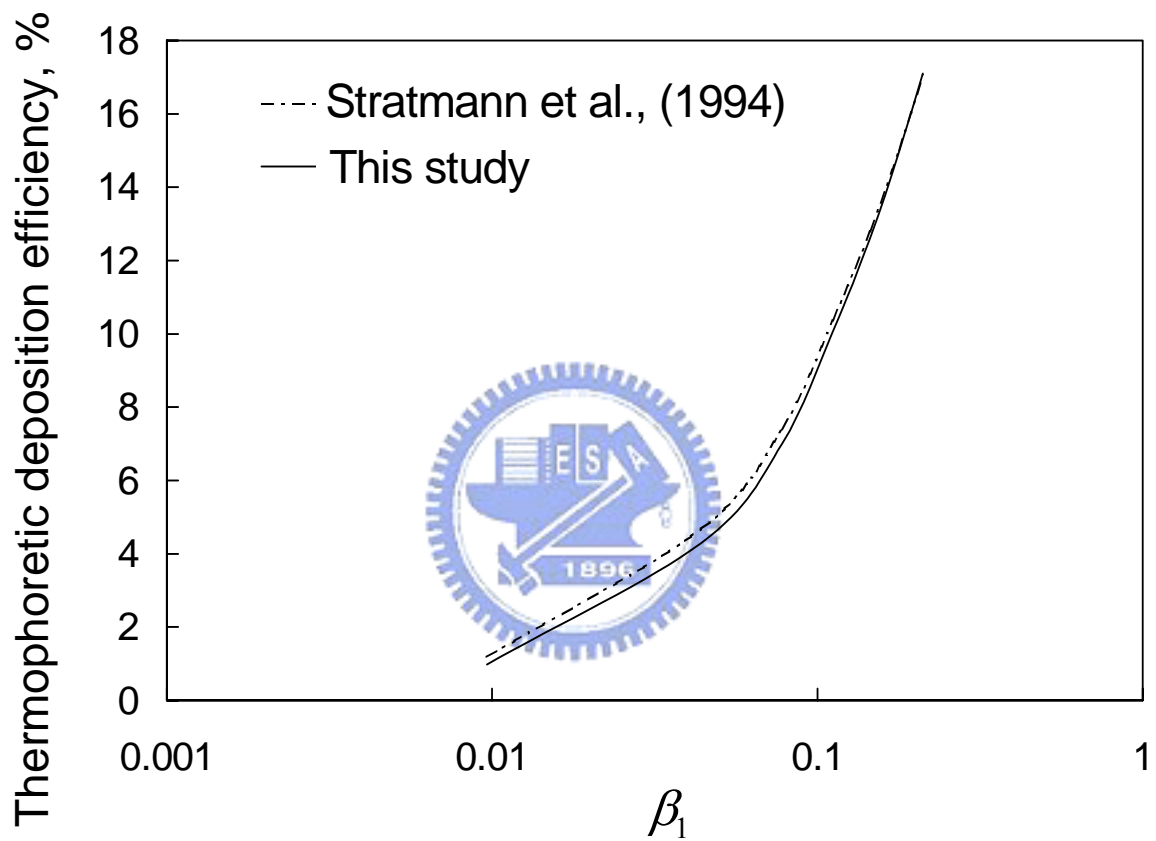


Figure 4.2 Comparison of present theoretical thermophoretic deposition efficiency with numerical prediction of Stratmann et al. (1994) in laminar tube flow.

4.2 Thermophoretic deposition efficiency for fully developed flow and developing temperature

When the flow is fully developed, the temperature could still be developing when there is a sudden temperature jump in the tube wall. The specific problem is as follows: The gas enters with a uniform particle concentration and temperature T_e and flow through a tube with a wall temperature equal T_e . At some distance far enough downstream such that the flow is fully developed, the wall temperature is decreased suddenly to T_w , which is different from T_e . This creates a “temperature jump” and the temperature field will start to develop from there. The developing temperature gradient in the radial direction is higher near the position of temperature jump, and the deposition efficiency is then expected to be higher than in the fully developed case.

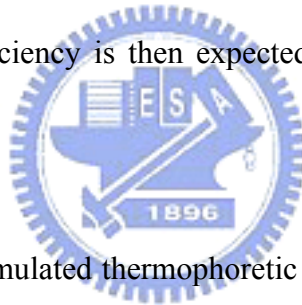


Fig. 4.3 shows that accumulated thermophoretic deposition efficiency calculated for the developing temperature case is higher than for the fully developed temperature case when the dimensionless distance from the entry, Z , is less than 5.0. Variable Z is defined as $Z = z/(0.05D_tPe_g)$, where z is the distance from the position of temperature jump, and $0.05D_tPe_g$ is the thermal entry length. It can be seen that the deposition efficiency increases from zero at the position of temperature jump, and approaches an asymptotic limit after Z is greater than about 5.0, when the temperature of hot gas approaches that of the tube wall. After Z becomes greater than 5.0, the deposition efficiencies for both cases are the same. Fig. 4.3 also shows that when θ^* is higher (T_e is close to T_w), the deviation of the deposition efficiency between developing temperature case and fully developed temperature case is smaller. For example, at $Z = 0.25$ and when θ^* equals to 2.70, the deviation is 37%; and when θ^* equals to 5.14,

the deviation is 20%.

4.3 Thermophoretic deposition efficiency for developing flow and developing temperature

Fig. 4.4 illustrates the effect of developing flow on the temperature distribution of a tube when θ^* equals 2.7. In order to make sure the simulated temperature field is correct, a fully developed velocity profile was first used to simulate the developing temperature field numerically, which is then compared with Graetz's analytical solution, Eq. (2.5). Good agreement seen in Fig. 4.4 indicates the present simulation is accurate. The simulated developing temperature profile based on the developing flow profile (Eq. (2.6)) shows that the temperature gradient close to the tube wall is higher than the case when the flow is fully developed, as depicted in Fig. 4.4.

Fig. 4.5 shows the accumulated thermophoretic deposition efficiency for a tube at different Z positions with $PrK_{th} = 0.31$ and $\theta^* = 5.14$ based on different numbers of grid points. As the resolution of the flow improves beyond 12,000, the deposition efficiency curves do not change appreciably. Therefore, 12,000 grids were used in the subsequent simulation.

Fig. 4.6 shows the effect of the developing velocity on the accumulated thermophoretic deposition efficiency at different θ^* values. It can be seen that the deposition efficiency approaches an asymptotic limit when the hot gas temperature is close to the tube wall, after Z is greater than about 5.0. For the combined developing case, the limiting value for the thermophoretic deposition efficiency of an infinite

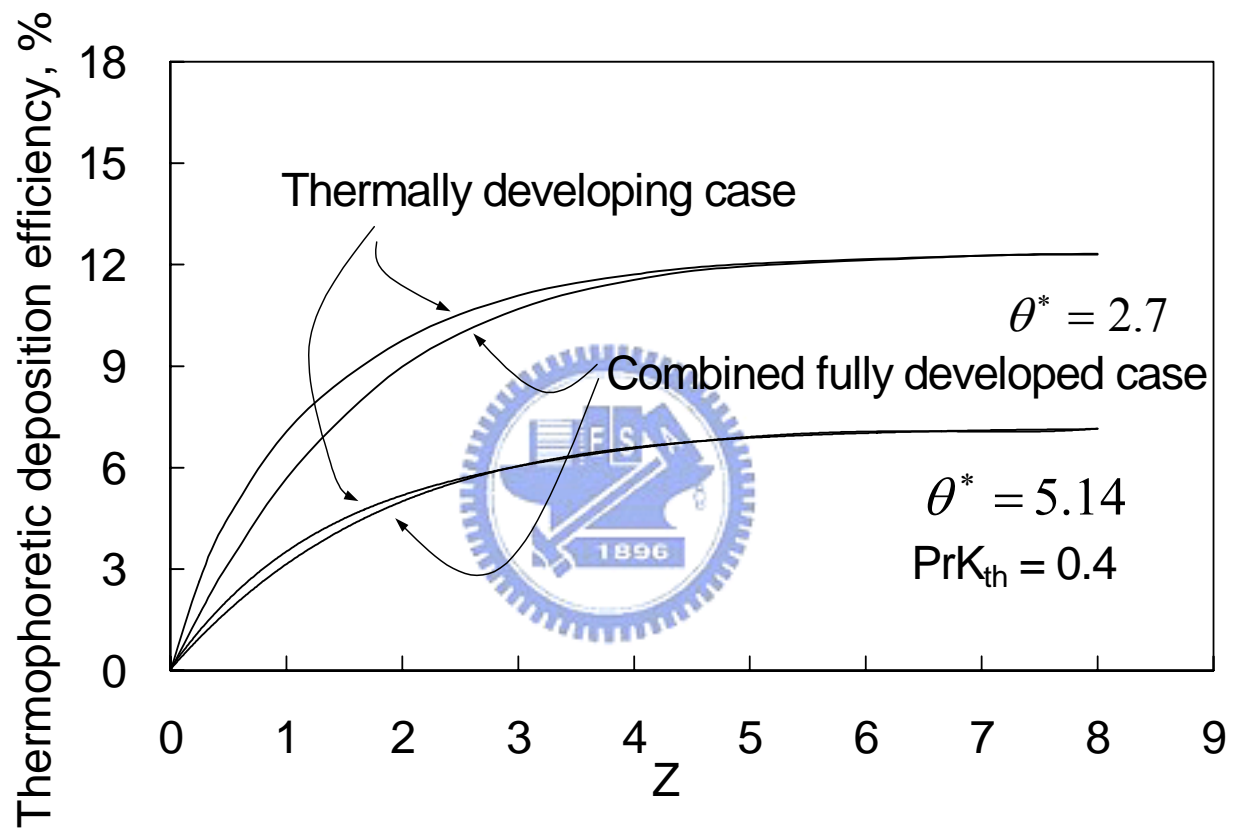


Figure 4.3 Comparison of accumulated thermophoretic deposition efficiency between different θ^* s versus Z , fully developed flow.

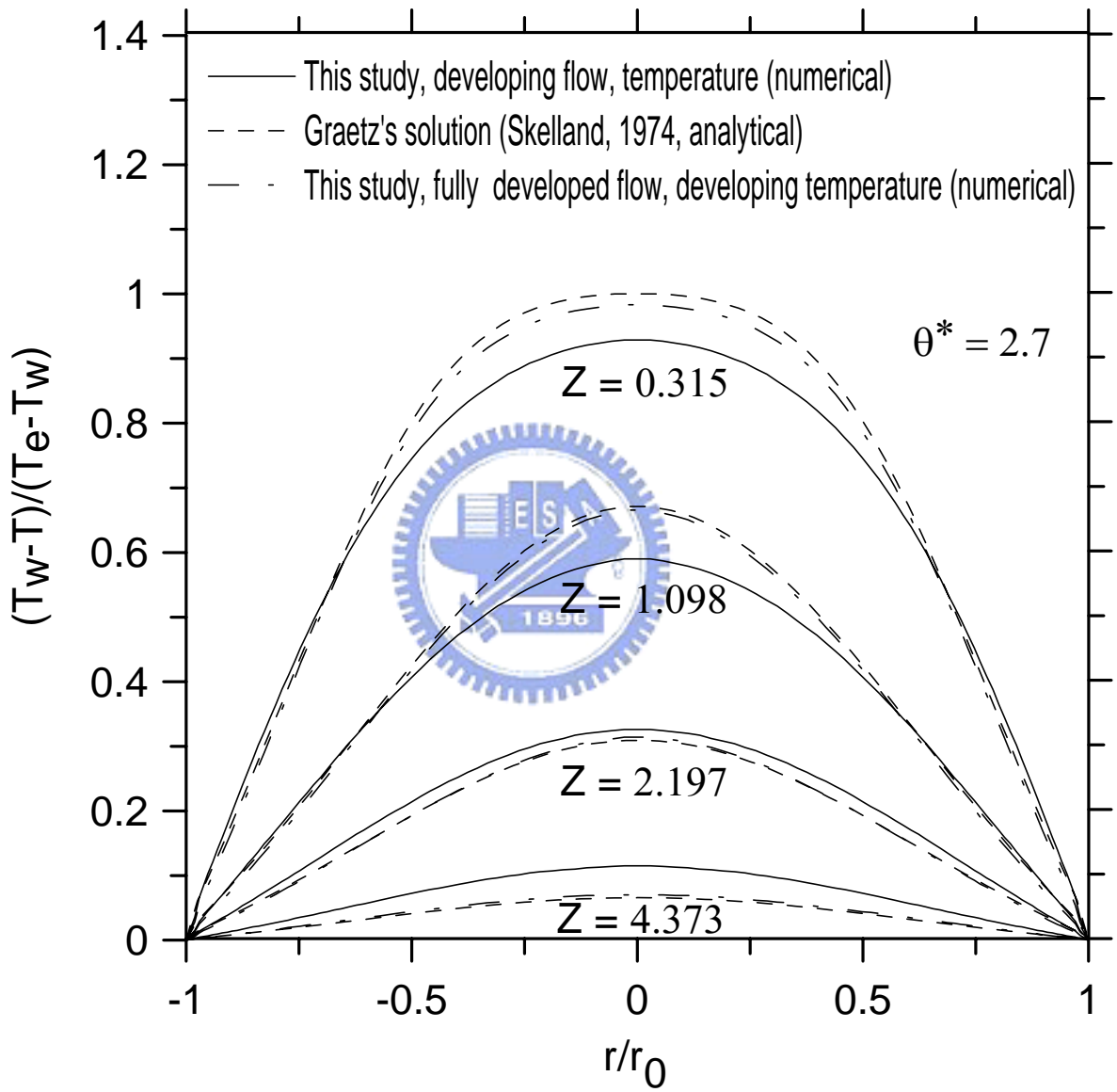


Figure 4.4 Dimensionless temperature profiles as a function of dimensionless radial and axial coordinates.

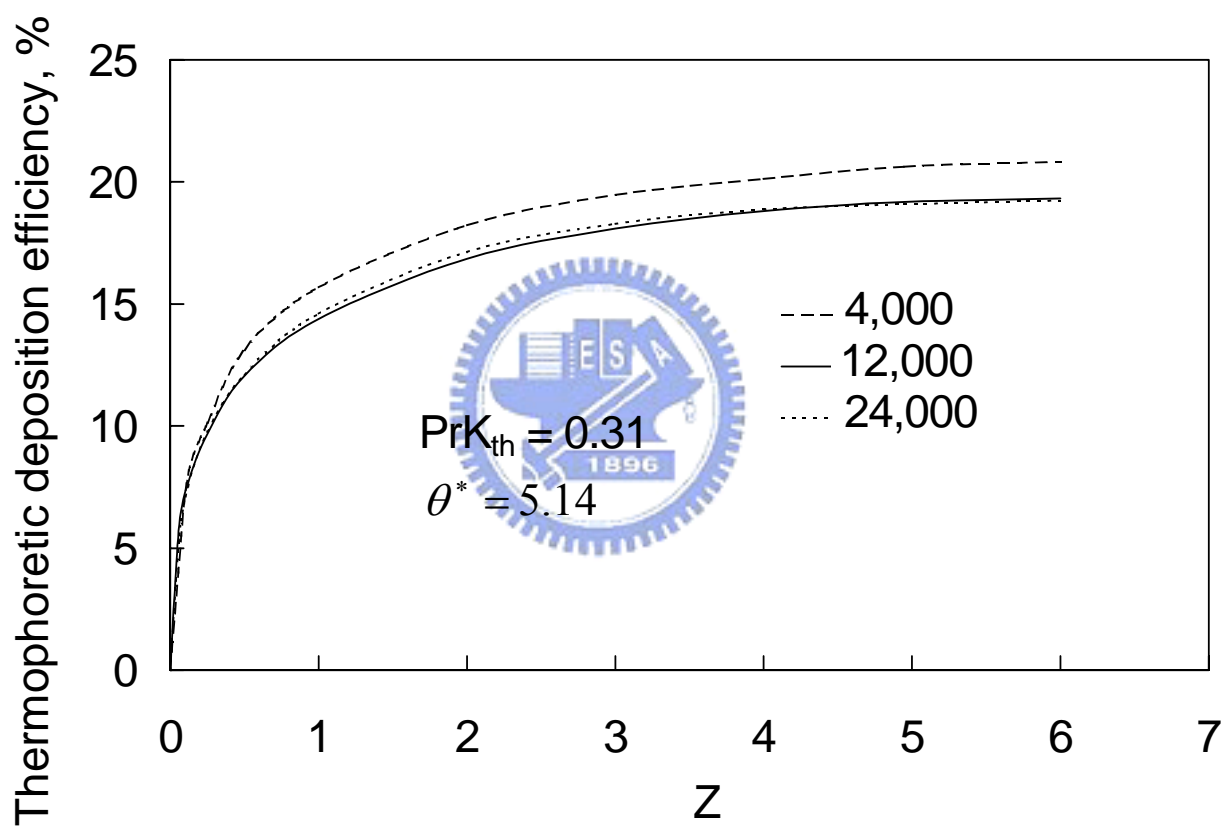


Figure 4.5 Accumulated thermophoretic deposition efficiency of aerosol particles using different numbers of grids, combined developing case.

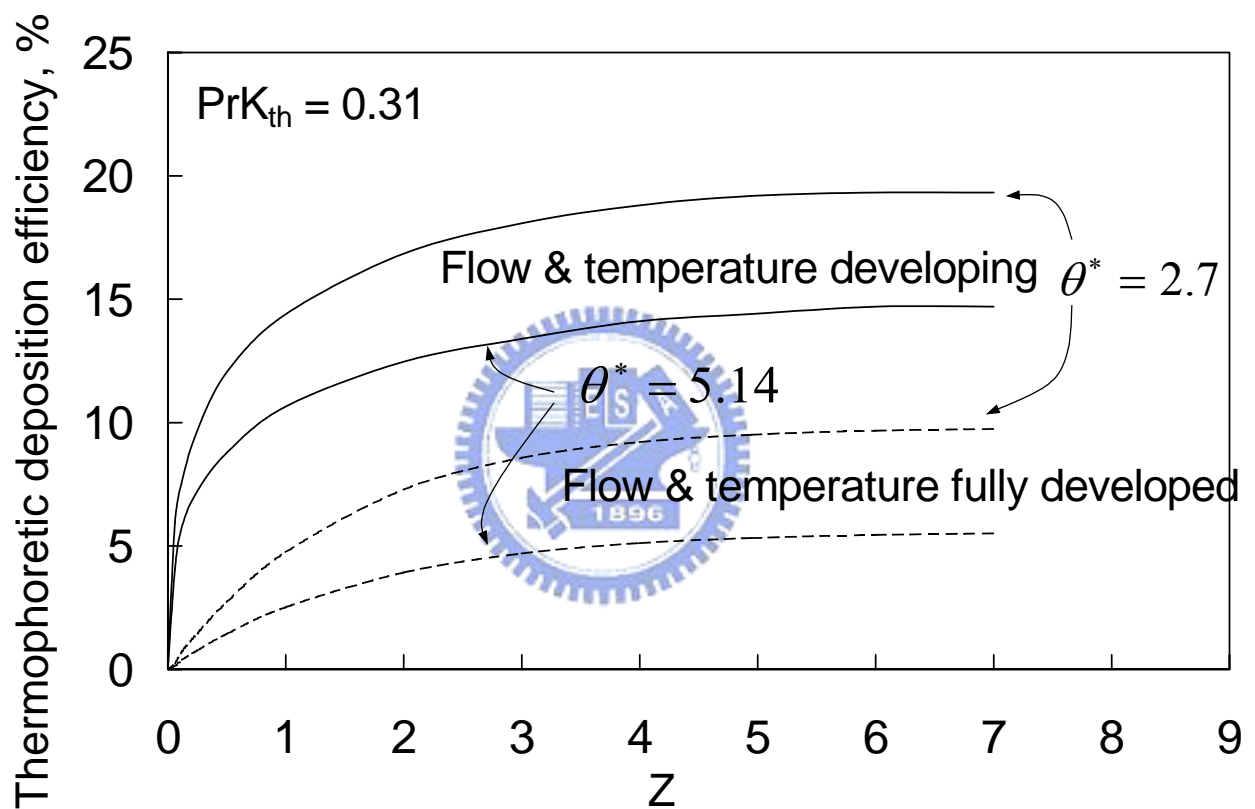
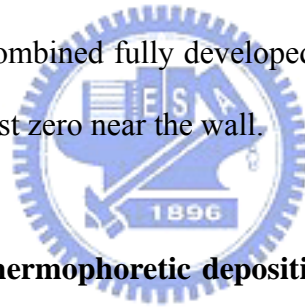


Figure 4.6 Comparison of accumulated thermophoretic deposition efficiency between different θ^* s versus Z.

Table 4.1 Accumulated thermophoretic deposition efficiency of combined developing case and combined fully developed case at different positions of a tube.

Z	Combined developing		Combined fully developed	
	R _c	Eff. (%)	R _c	Eff. (%)
0.06	0.9698	5.96	0.9689	0.37
0.12	0.9610	7.64	0.9561	0.74
0.25	0.9504	9.67	0.9373	1.48
0.50	0.9378	12.05	0.9132	2.76
1.00	0.9253	14.39	0.8836	4.81
2.00	0.9119	16.85	0.8534	7.38
3.00	0.9051	18.08	0.8691	8.40
4.00	0.9011	18.80	0.8333	9.34
4.95	0.8990	19.19	0.8304	9.64
6.00	0.8982	19.32	0.8288	9.80

long tube is higher than the combined fully developed case. For example, when PrK_{th} equals 0.31 and θ^* equals 2.7, the deposition efficiencies are 19.3 % and 9.8 %, respectively. Table 4.1 gives a list of the critical radial position and the corresponding accumulated thermophoretic deposition efficiency of the combined developing and combined fully developed cases when $PrK_{th} = 0.31$ and $\theta^* = 2.7$. It shows that the critical radial position of the combined developing case is larger than that of the combined fully developed case indicating that the inward radial velocity tends to increase r_c and reduce deposition efficiency. And the effect of inward radial velocity is larger than the increase of thermal gradient near the inlet on the position of r_c . However since both the flow velocity and particle concentration are uniform at the tube entrance for the combined developing case, the resulting deposition efficiency is larger than the combined fully developed case in which the velocity and hence the particle flux is almost zero near the wall.



4.4 Empirical equation of thermophoretic deposition efficiency for the case of a long tube

The thermophoretic deposition efficiency is a unique function of the dimensionless parameter β_1 . Fig. 4.7 shows such this relationship; correlation equations are also indicated.

It can be seen from Eq. (A.6) that particle transport due to combined convection and thermophoresis depends on three parameters, the product of the Prandtl number and thermophoretic coefficient, PrK_{th} , the dimensionless temperature $(T_e - T_w)/T_e$ and the gas Peclet number Pe_g . The thermophoretic deposition efficiency is shown independent on the gas Peclet number by Walker et al. (1979), but only on the

thermophoretic parameter β_1 , which is

$$\beta_1 = \text{Pr} K_{th} \frac{T_e - T_w}{T_w} \quad (4.1)$$

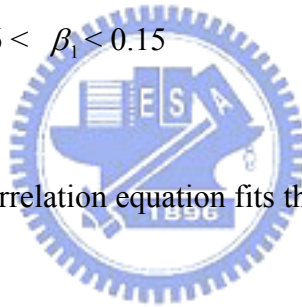
In this study, the empirical equation for the combined fully developed is found to be

$$\eta_f = 0.783\beta_1^{0.94}, \quad 0.007 < \beta_1 < 0.19 \quad (4.2)$$

and for the combined developing case, the empirical equation is found to be

$$\eta_d = 0.549\beta_1^{0.48}, \quad 0.006 < \beta_1 < 0.15 \quad (4.3)$$

Fig. 4.7 also shows that the correlation equation fits the present numerical results very well.



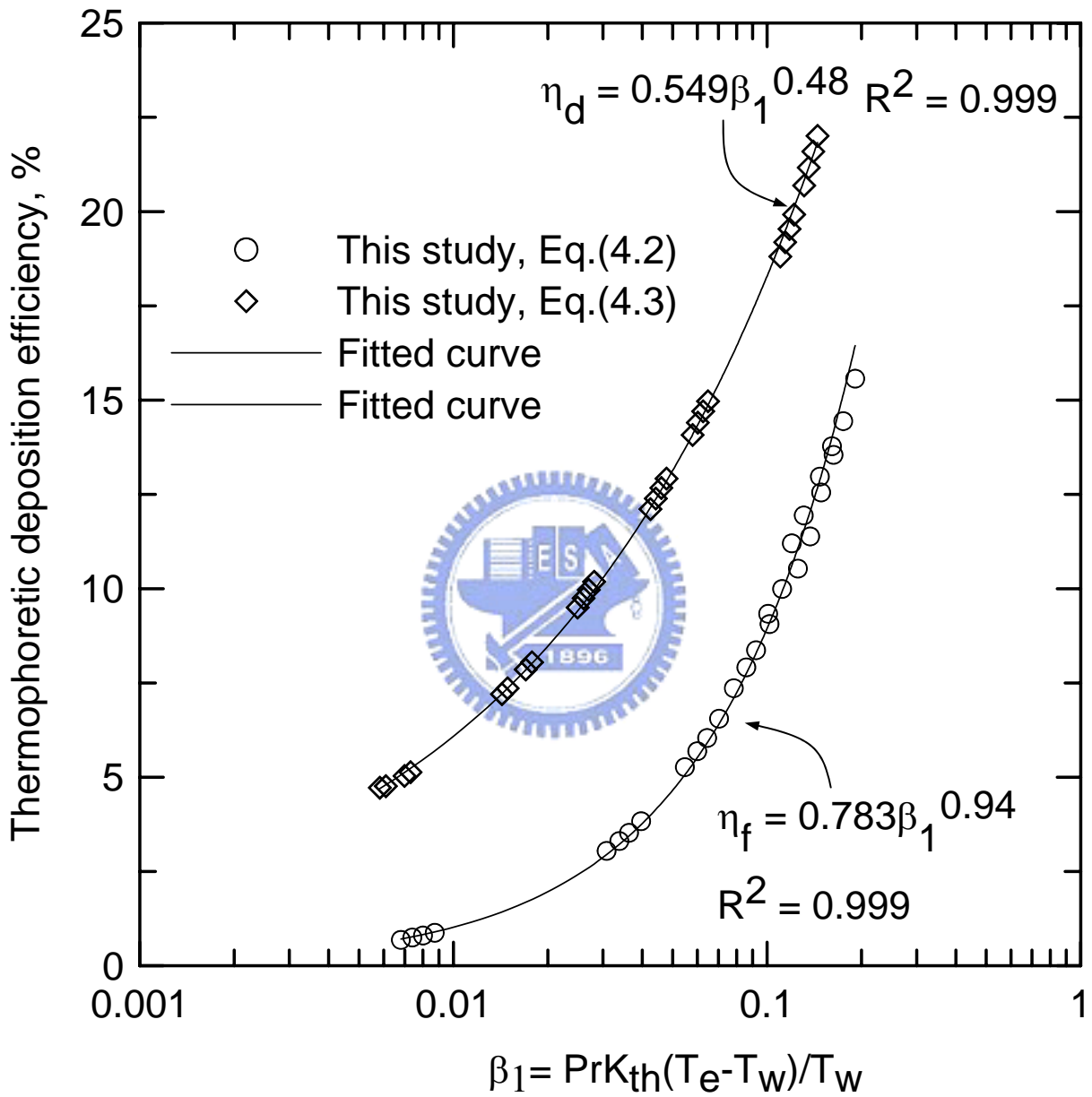


Figure 4.7 Thermophoretic deposition efficiency as a function of thermophoretic parameter β_1 in laminar fully developed flow and developing flow.

CHAPTER 5

EXPERIMENTAL RESULTS OF THE THERMOPHORETIC DEPOSITION EFFICIENCY

5.1 Particle deposition efficiency due to isothermal deposition mechanisms

In laminar tube flow, particles may be deposited in the tube due to Brownian diffusion and electrostatic deposition. The experiment was done when both the aerosol stream and tube wall were kept at the same temperature, 296 K, in the laminar flow condition (4 l min^{-1}) so that there was no thermophoretic deposition. The theoretical diffusional deposition efficiencies are compared with the experimental data for charge neutral particles and particles in Boltzmann charge equilibrium in Fig. 5.1. The error bars in the figure indicate that the relative standard deviations of the data points are about $\pm 20\%$.



The results in Fig. 5.1 show that the experimental data are about 2.2 % higher than the theoretical diffusional deposition efficiencies for particles in Boltzmann charge equilibrium and when the particle diameter is less than $0.15 \mu\text{m}$, and the deviation increases the decreasing particle size with the maximum of about 3.8 % for $0.038 \mu\text{m}$ particles. For charge neutral particles, the experimental data are very close to the theoretical diffusional deposition efficiencies, and the absolute differences are less than 0.65 % for all particle sizes. That is, it is important to consider electrostatic deposition even for particles that are in Boltzmann charge equilibrium in view that the experimental thermophoretic deposition efficiencies are small, which are generally less than 10 % in this study.

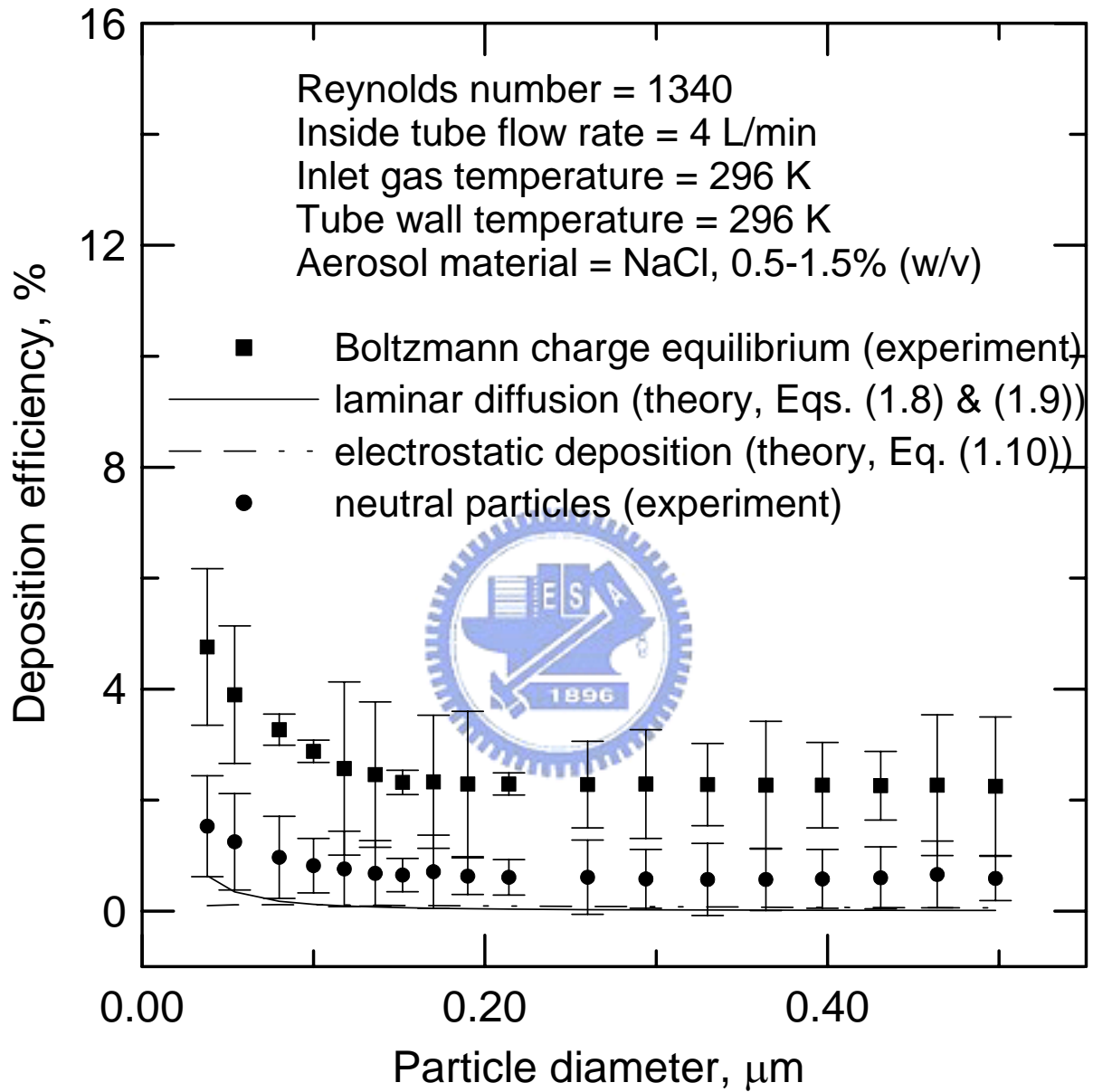


Figure 5.1 Comparison of experimental deposition efficiencies (isothermal) and theoretical predictions of diffusional and electrostatic deposition under laminar flow conditions, ($Re = 1340$).

The electrostatic deposition efficiencies as a function of particle diameter for particles in Boltzmann charge equilibrium are also shown in Fig. 5.1. It can be seen that the theoretical efficiency is indeed very small compared to the experimental data and it warrants further theoretical study on the deposition due to particle electrostatic.

Particles deposition in turbulent tube flow may be due to eddy diffusion and turbulent inertial deposition. The penetration efficiency, P_{tur} , is computed using Eqs. (1.16) and (1.17). The particle deposition efficiency including both eddy diffusion and turbulent deposition in turbulent tube flow is calculated as

$$\eta_t = 1 - (P_{d,t} \times P_{tur}) \quad (5.4)$$

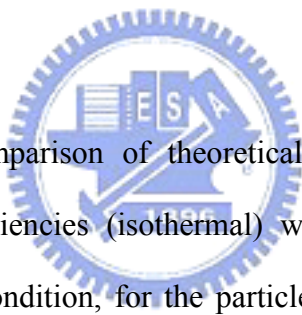


Fig. 5.2 shows the comparison of theoretical results based Eq. (5.4) with experimental deposition efficiencies (isothermal) with error bars indicated under turbulent flow (20 l min^{-1}) condition, for the particle diameter ranging $0.038\text{-}0.498 \text{ }\mu\text{m}$. The graph illustrates that the experimental efficiencies are about 3.5 % higher than the theoretical efficiencies for particles in Boltzmann charge equilibrium. But for neutral particles, particle deposition efficiencies are lower and agree very well with the theoretical predictions. Again, the electrostatic deposition for particles in Boltzmann charge equilibrium is seen to be important and must be accounted for. It is best if one could use neutral particles for an accurate thermophoretic deposition experiment without the interference from electrostatic deposition. Also the calculation shows that the deposition due to turbulent inertial deposition is much smaller than that due to eddy diffusion. The deposition efficiency due to turbulent inertial deposition increases only slightly from 0.0 % for $0.038 \text{ }\mu\text{m}$ particles with the

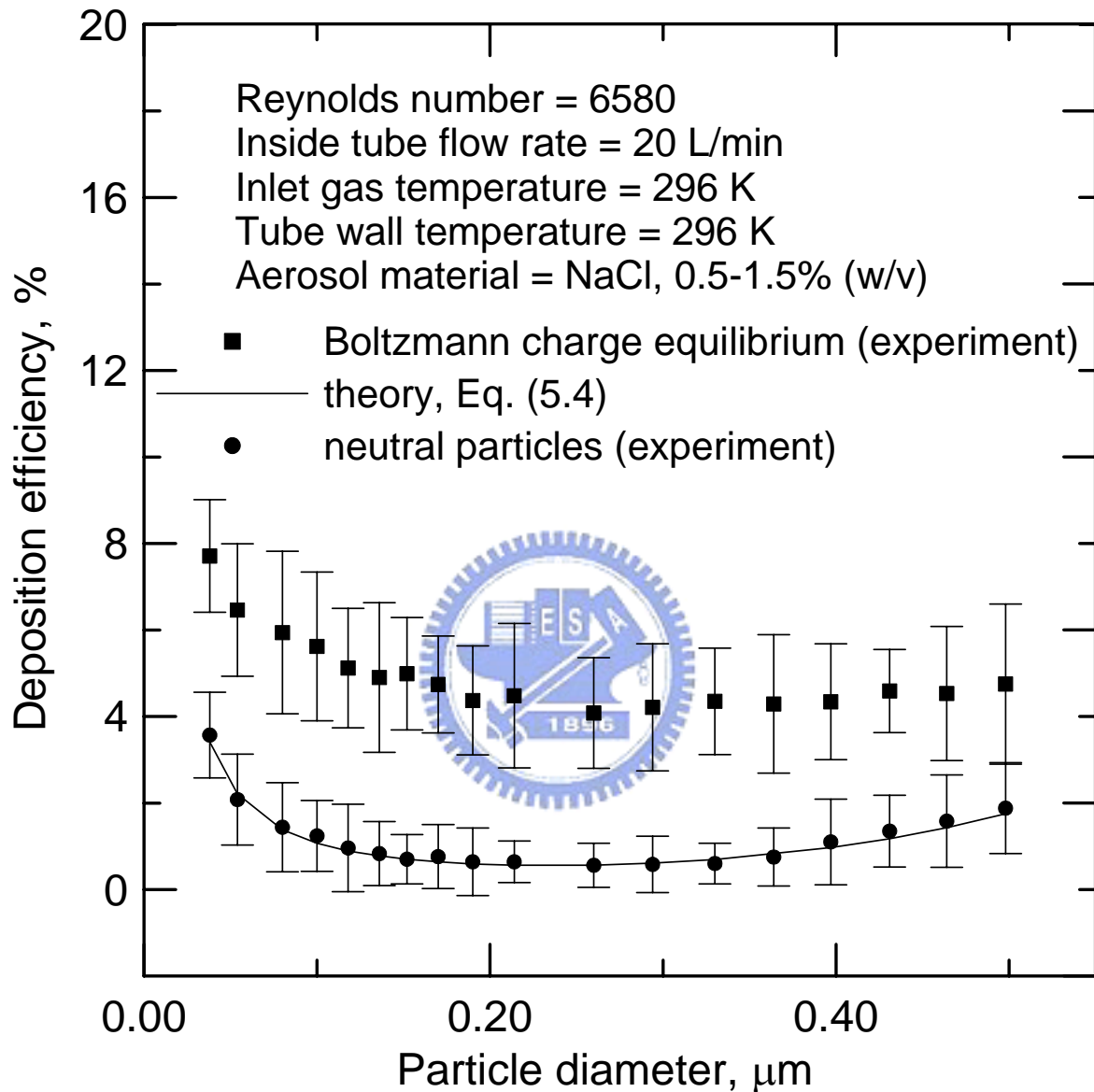
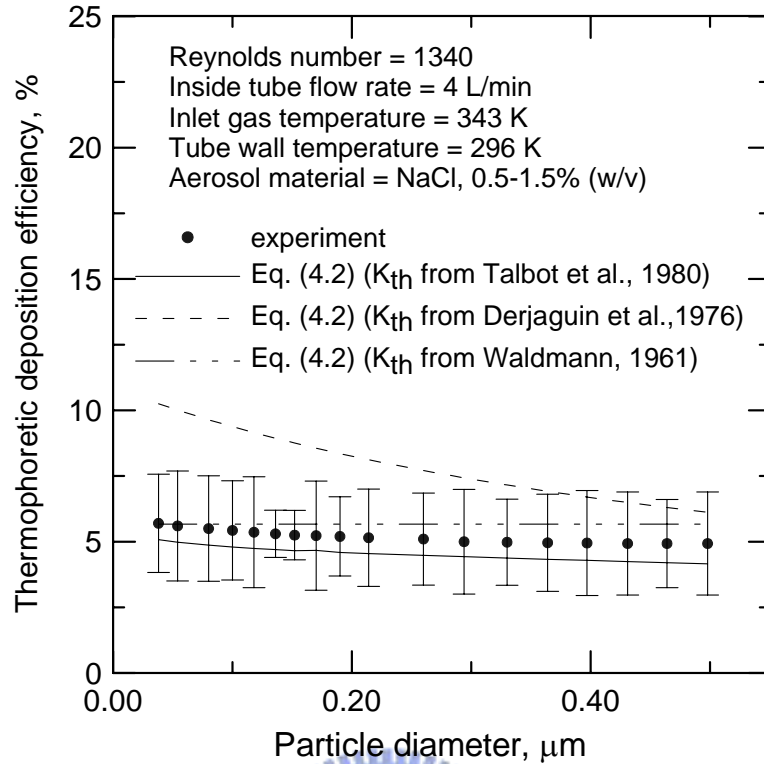
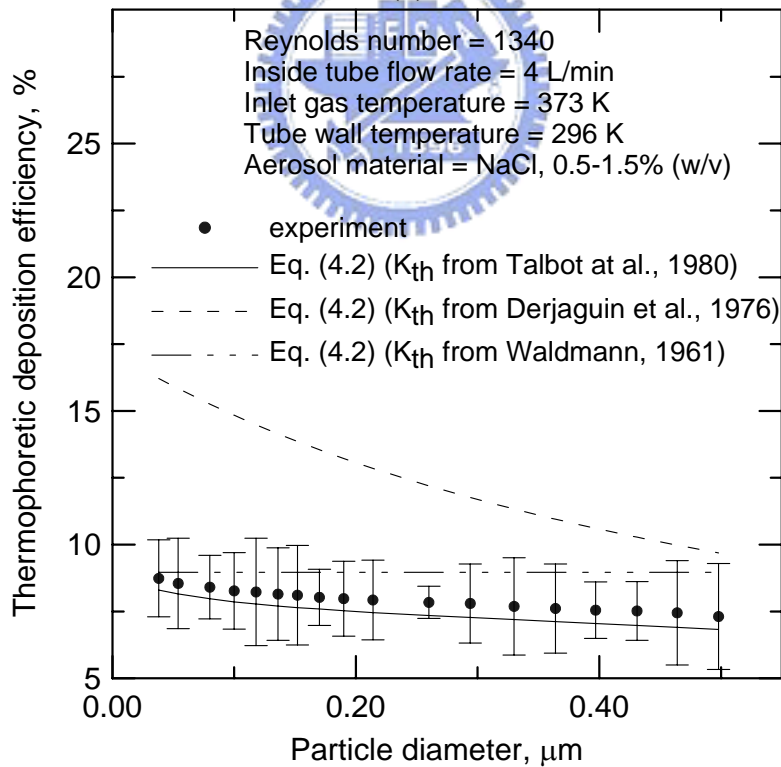


Figure 5.2 Comparison of experimental deposition efficiencies (isothermal) and theoretical predictions of combined turbulent diffusion and inertial deposition under turbulent flow conditions ($Re = 6580$).



(a)



(b)

Figure 5.3 Comparison of experimental data and theoretical predictions of thermophoretic deposition efficiency of combined fully developed case under laminar flow conditions. (a) $Re = 1340$, $T_e = 343$ K (b) $Re = 1340$, $T_e = 373$ K.

increasing particle diameter to a maximum value of about 0.5 % for the particle of 0.498 μm in diameter.

5.2 Thermophoretic deposition efficiency

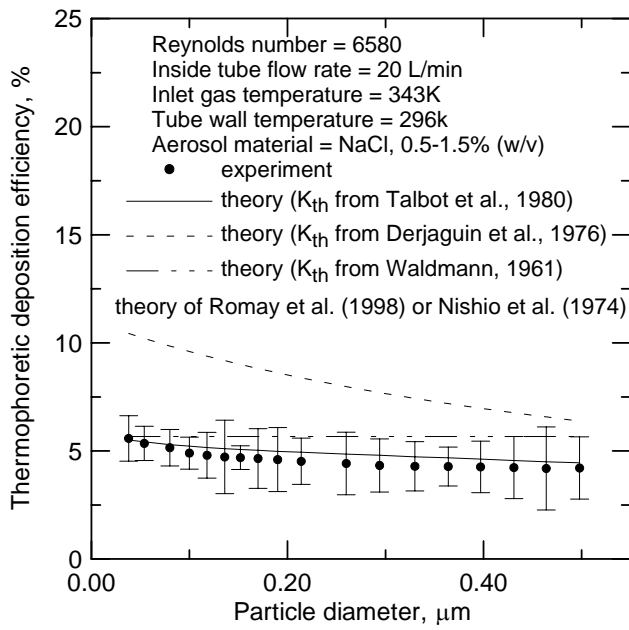
Figs. 5.3(a) and (b) show that in laminar flow condition, experimental thermophoretic deposition efficiencies (with error bars) at 343 K and 373 K, after excluding isothermal deposition efficiencies, are in good agreement with the theoretical predictions, Eq. (4.2), with the thermophoretic coefficient suggested by Talbot et al. (1980). The theoretical coefficient of Derjaguin et al. (1976) leads to the overestimation of the thermophoretic deposition efficiency in the range of particle sizes tested. Figures also show that the thermophoretic deposition efficiency increases with an increasing inlet gas temperature. The theoretical efficiency based on the thermophoretic coefficient of Waldmann (1961) is nearly a horizontal line, indicating it is independent of particle size. The theoretical predictions based on the coefficient of Waldmann (1961) are higher than the experimental data and they agree only when the particle size is smaller than 0.038 μm .

In the turbulent flow regime, Fig. 5.4(a) again shows that the experimental thermophoretic efficiencies (with error bars, at 343 K) are very close to the theoretical values based on the thermophoretic coefficient of Talbot et al. (1980) (flow rate equals 20 l min^{-1}). When the flow rate is increased further to 32 l min^{-1} (Fig. 5.4(b) and (c)), the experimental thermophoretic deposition efficiencies are still in very good agreement with theoretical predictions based on the coefficient of Talbot et al. (1980), despite that the reading of the CNC becomes more fluctuating. Fig. 5.4(c) shows that when inlet gas temperature is increased to 398 K, the experimental

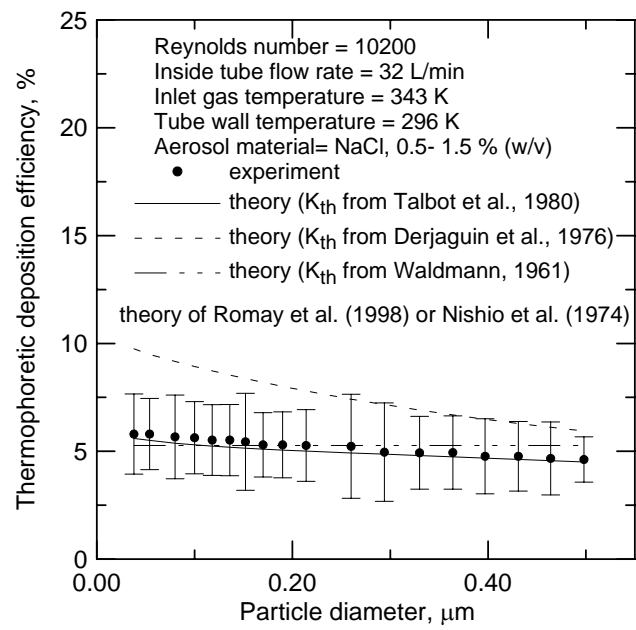
thermophoretic deposition efficiency of this study is close to the theoretical prediction of Romay et al. (1980) after excluding other deposition mechanisms such as turbulent diffusion, inertial deposition and particle electrostatic charge. The experimental data were again compared with the theoretical predictions of Romay et al. (1998) and Nishio et al. (1974) in Fig. 5.5 for particles of 0.5 and 0.498 μm at $\text{Re}=10200$. It can be seen that the experimental data agree very well with both theories.

In Fig. 5.6(a) the thermophoretic coefficient derived from the experimental data of thermophoretic deposition efficiency is plotted as a function of the Knudsen number, $2\lambda/d_p$, in the laminar flow regime. It shows that the present experimental data agree well with the theory of Talbot et al. (1980). The relative standard deviations of the data points are less than $\pm 20\%$. The filled squares illustrate the experimental data of inlet gas temperature at 343 K and filled circles are the experimental data at 373 K in laminar flow conditions. The dashed horizontal line represents the constant value of K_{th} , 0.55, by Waldmann (1961) for the free molecular flow regime ($\text{Kn} \gg 1$). The present data approach Waldmann's free molecular limit as Kn is greater than about 3.0.

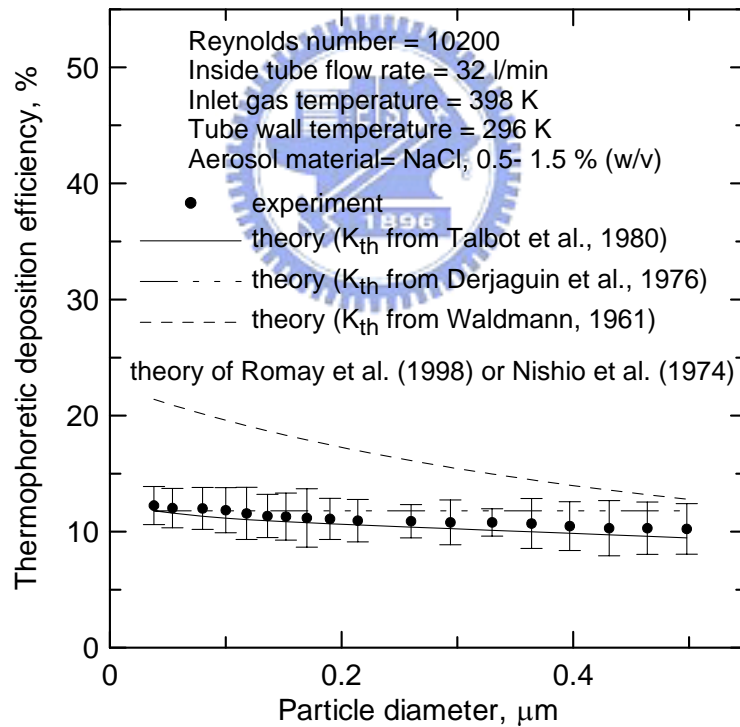
In the turbulent flow regime, Fig. 5.6(b) also illustrates that the thermophoretic coefficient developed by Talbot et al. (1980) is much more accurate than that of Derjaguin et al. (1976) and Waldmann (1961). The relative standard deviation of the data points is less than $\pm 23\%$. It also indicates that Waldmann's thermophoretic coefficient is applicable when Kn is greater than about 3.



(a)



(b)



(c)

Figure 5.4 Comparison of experimental data and theoretical predictions of thermophoretic deposition efficiency of Romay et al. (1998) under turbulent flow conditions. (a) $Re = 6580$, $T_e = 343K$ (b) $Re = 10200$, $T_e = 343K$. (c) $Re = 10200$, $T_e = 398K$.

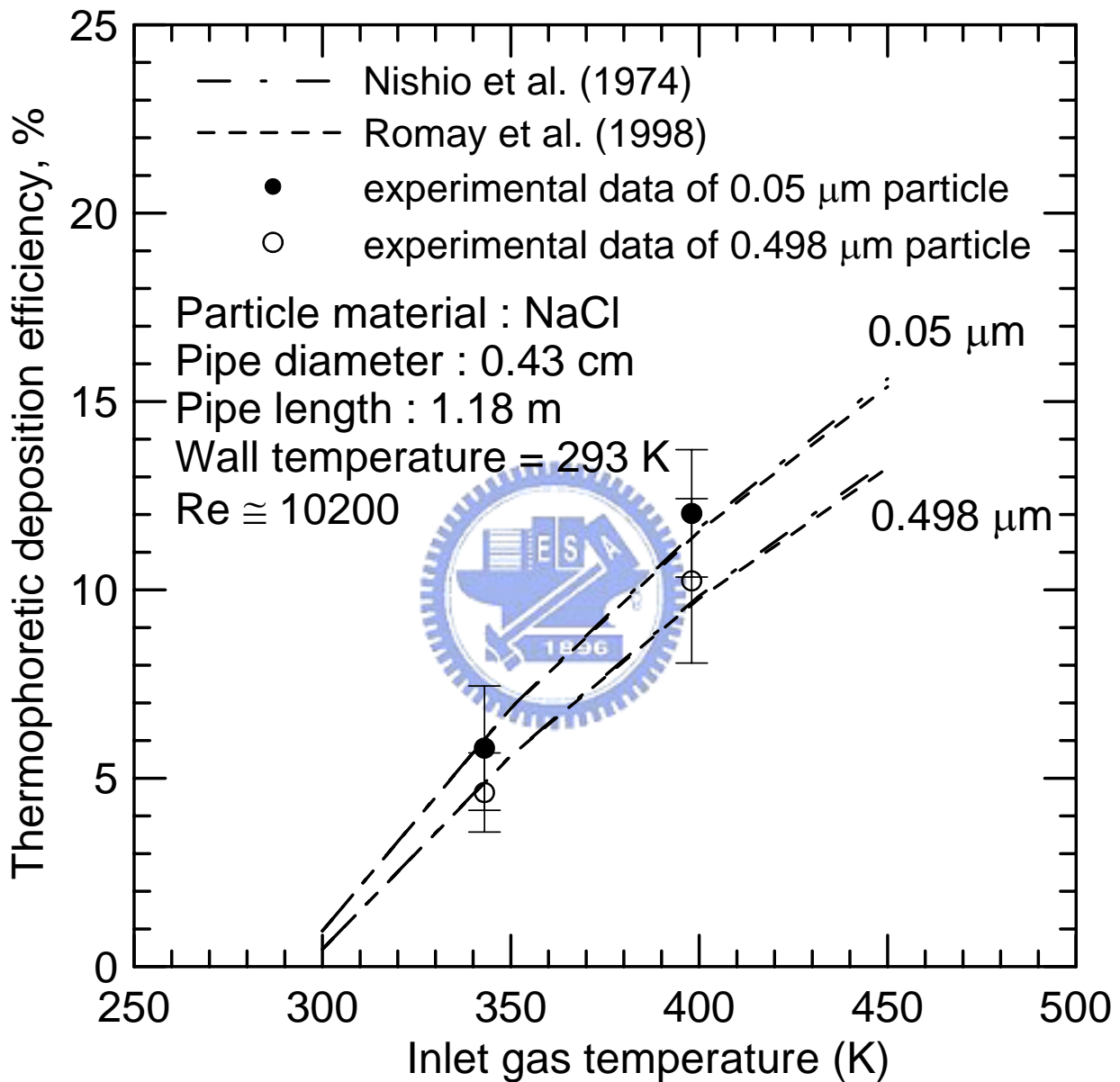
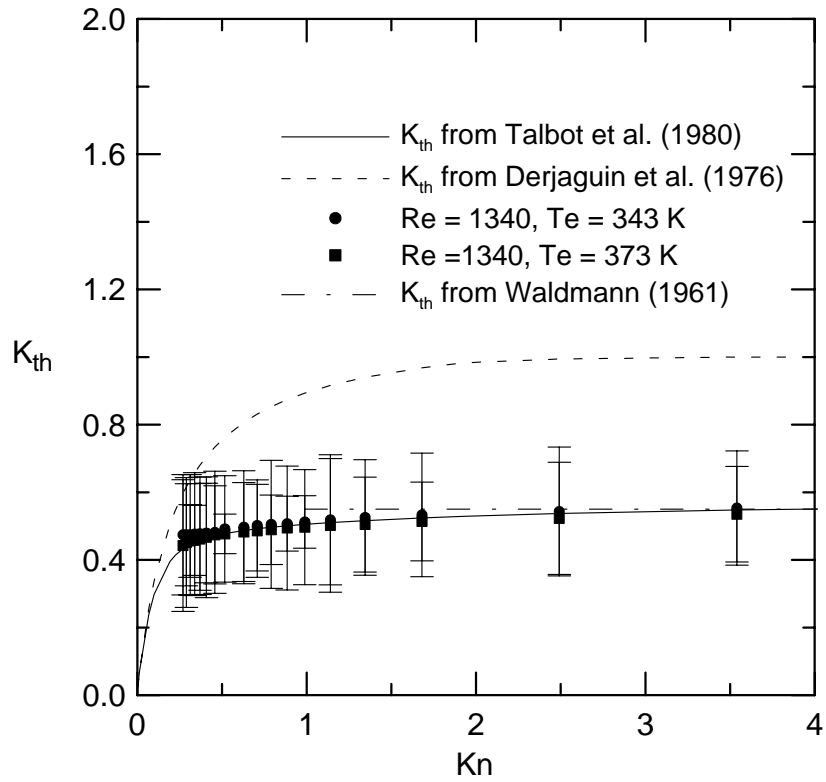
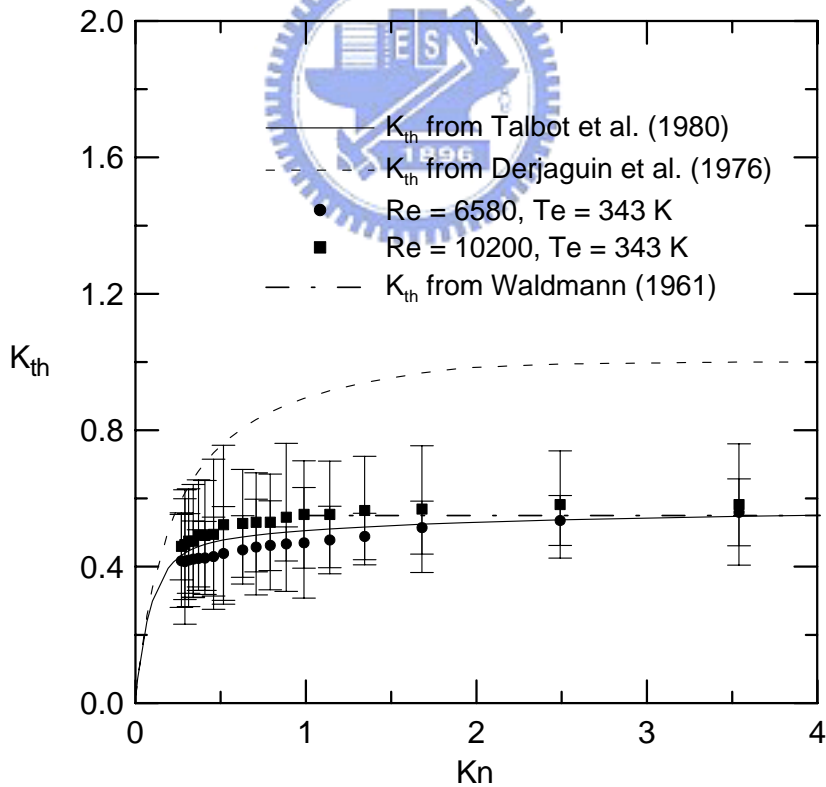


Figure 5.5 Comparison of theoretical predictions ($Re = 10200$) for particles of 0.05 and 0.498 μm in diameter in turbulent flow.



(a)



(b)

Figure 5.6 Comparison of experimental thermophoretic coefficients K_{th} with theories. Experimental K_{th} is calculated based on experimental data and theoretical thermophoretic deposition efficiency in (a) laminar flow (b) turbulent flow.

CHAPTER 6

SUPPRESSION OF PARTICLE DEPOSITION BY THERMOPHORESIS

The particle convection-diffusion equation, Eq. (2.15), without considering thermophoresis was solved and the numerical diffusional efficiency was compared with Gormley and Kennedy equation (in Baron and Willeke, 2001). This is the so-called isothermal case when the tube wall and inlet gas flow temperatures are the same. Fig. 6.1 shows the particle deposition efficiency as a function of the dimensionless deposition parameter, $\mu' = \pi DL/Q$, based on different numbers of grids. It is seen that the numerical method is able to predict the particle deposition efficiency due to convection-diffusion in a tube flow very well. At the grid number of 12,000, the calculated deposition efficiency was found to be accurate and deviate from the analytical value by a maximum of 1.9% only.

6.1 Thermophoretic deposition efficiency for tube wall temperature lower than that of gas flow

To make sure that the present numerical study is accurate, the thermophoretic deposition efficiency was calculated based on fully developed flow assumption. The simulated thermophoretic deposition efficiency in laminar tube flow shown in Fig. 6.2 illustrates that the present numerical results agree with the exact solution of Walker et al. (1979) or semi-empirical equation of Eq. (4.2). The approximate equation of Walker et al. (1979) underestimated the thermophoretic deposition efficiencies, as given in the Table 1.1. Hence, both the isothermal convection-diffusion results in the last section, and thermophoretic deposition efficiency results in this section demonstrate that the present numerical simulation is accurate.

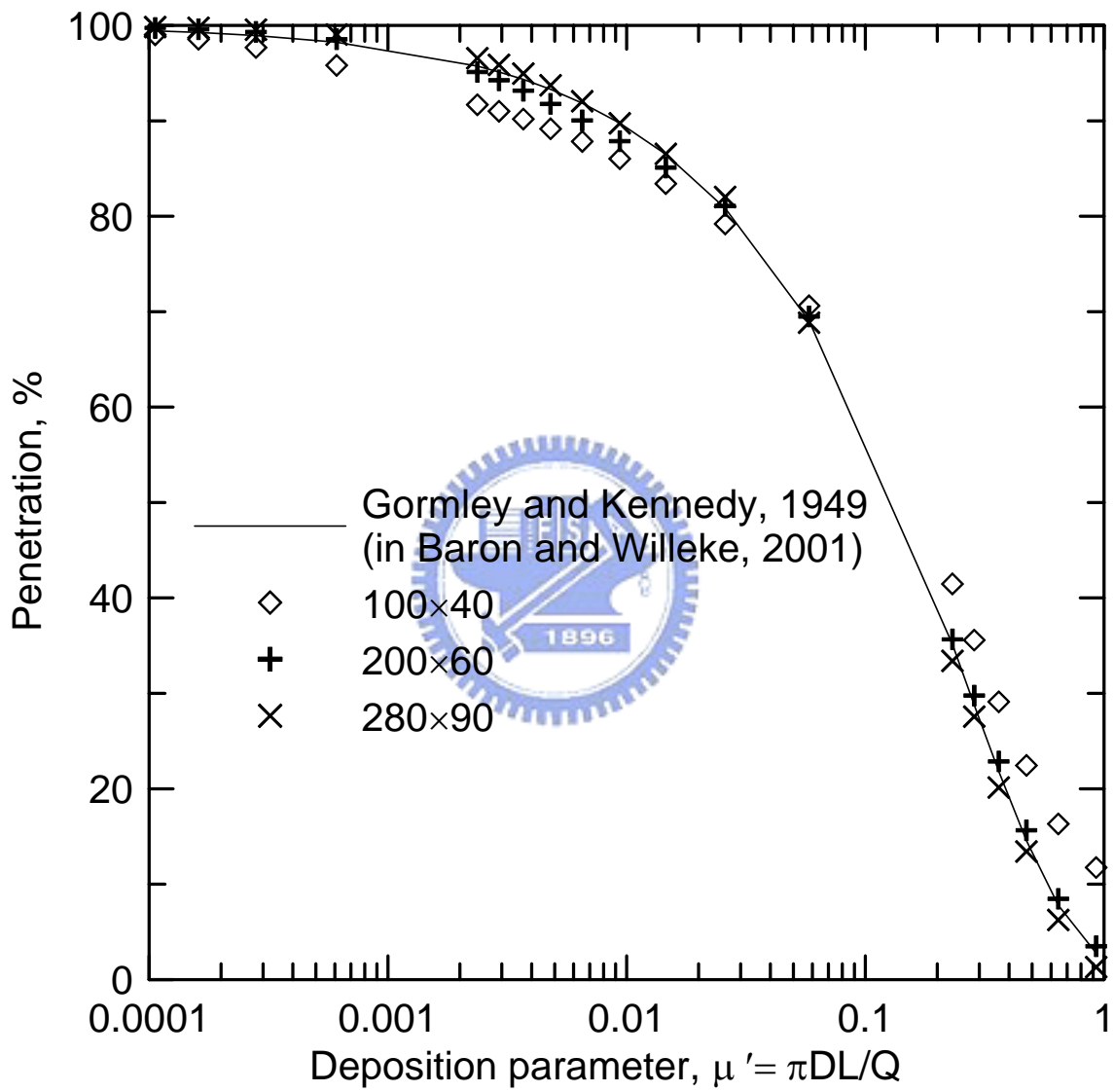


Figure 6.1 Particle deposition efficiency as a function of dimensionless parameter, $\mu' = \pi DL/Q$, for isothermal case.

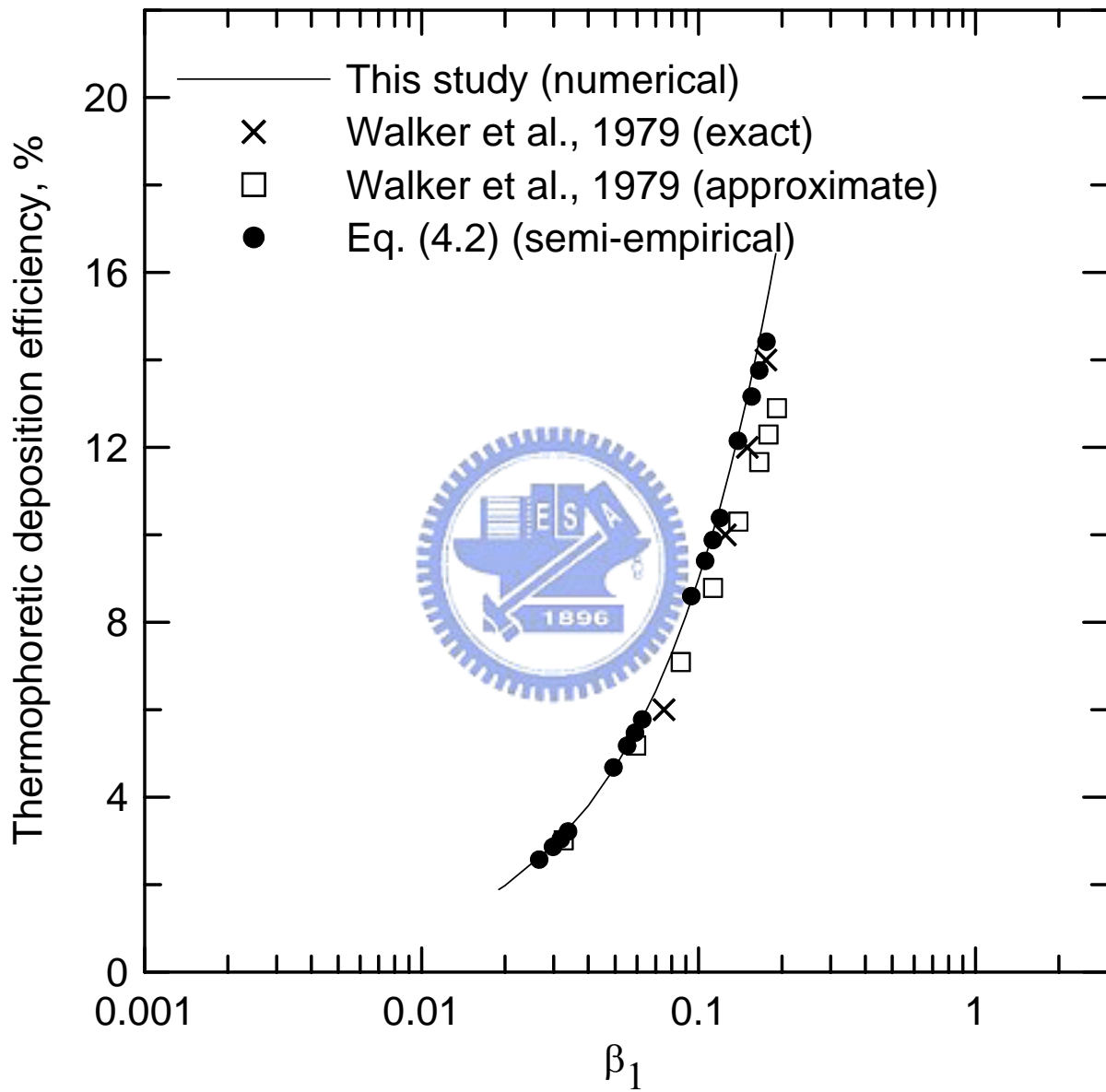


Figure 6.2 Dimensionless temperature profiles as a function of dimensionless radial and axial coordinates.

6.2 Effect of temperature difference between the tube and gas flow on the particle deposition efficiency

Effect of heating up the tube wall on reducing particle deposition efficiency was studied both numerically and experimentally. The inlet air flow temperature at the experimental section was kept constant at 296 K while the tube wall temperature was increased from 296 to 315 K. Three aerosol flow rates of 2, 3 and 5 slpm with the corresponding Reynolds number of 640, 960 and 1600, respectively, were tested using particles ranging from 0.01 to 0.04 μm in diameter. Figs. 6.3(a)-(c) show the comparison between the numerical and experimental results for NaCl particles with the diameter of 0.01, 0.02 and 0.04 μm , respectively. The experimental data show good agreement with numerical results in these figures. It is seen that for a given particle diameter, the particle deposition efficiency is decreased with an increasing tube wall temperature and gas flow Reynolds number. Reduction of deposition efficiency is very steep when the tube wall is only several degrees higher than the air flow temperature. The deposition of particle is suppressed completely (or zero deposition efficiency) when the tube wall is heated to a temperature high enough so that diffusional force is overcome by thermophoretic force.

Fig. 6.3(a) illustrates that the numerical results of a 0.01 μm NaCl particle at charge neutral condition, the numerical particle deposition efficiencies are 9.39, 7.19 and 4.88 % at the corresponding gas flow rate of 2, 3 and 5 slpm, respectively, when the tube wall temperature is kept at 296 K. These are laminar diffusion efficiencies. Further increasing the tube wall temperature to 320, 315 and 312 K for the gas flow rate of 2, 3 and 5 slpm, respectively, the particle deposition efficiency will drop to zero.

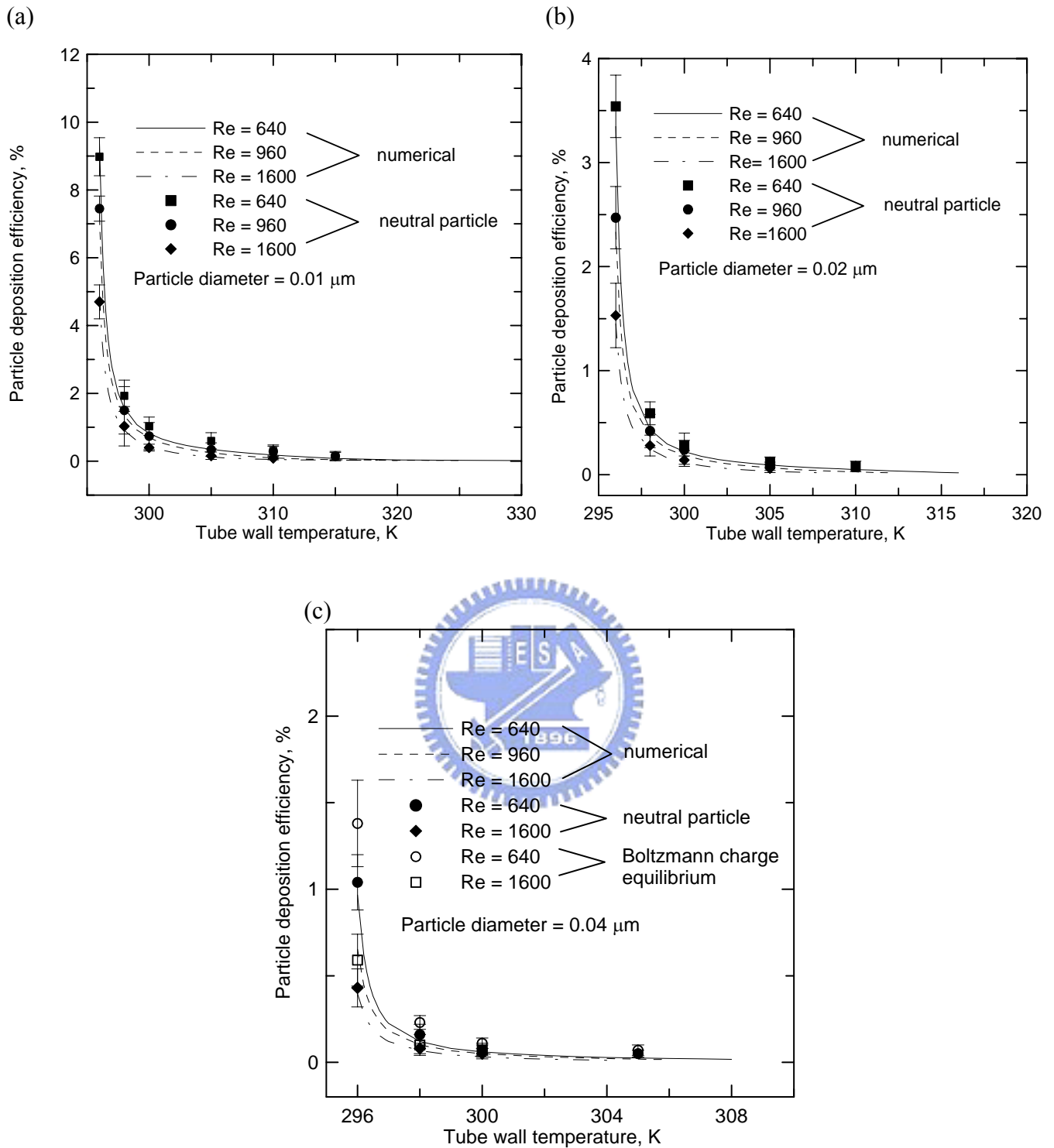


Figure 6.3 Particle deposition efficiency versus tube wall temperature for NaCl particles with particle diameter of (a) 0.01 μm (b) 0.02 μm (c) 0.04 μm . The test tube length and inner diameter are 1.18 and 0.0043 m, respectively, and the inlet air temperature is 296 K.

Increasing the particle diameter to 0.02 μm or 0.04 μm , similar effect of wall temperature on reducing deposition efficiency can be observed in Figs. 6.3(b) and (c). For 0.02 μm particles (Fig. 6.3(b)) and when tube wall is kept at 296 K, the numerical particle deposition efficiencies are 3.35, 2.33 and 1.45 % at the gas flow rate of 2, 3 and 5 slpm, respectively. Zero particle deposition efficiency occurs at the tube wall temperature of 312, 308 and 305 K for the gas flow rate of 2, 3 and 5 slpm, respectively. For 0.04 μm particles (Fig. 6.3(c)), zero particle deposition efficiency occurs as the tube wall is increased to 304, 302 and 300 K for the gas flow rate of 2, 3 and 5 slpm, respectively. That is, increasing the particle diameter will reduce the convection-diffusion strength of particles, and hence the required wall temperature for zero deposition is also decreased.

The above data are for completely charge neutral particles. For particles in Boltzmann charge equilibrium, the experimental results for 0.04 μm particles are shown in Fig 6.3(c), which shows that deposition efficiency is slightly higher (less than 0.34 % in average) than that of charge neutral particles. This is due to the image force exerted on the particles that carry charges. The calculated particle deposition efficiency, from Eqs. (1.13) and (1.14), due to image force for a singly charged particle is 0.057 % (Re=1600) or 0.059 % (Re=640) when the tube wall temperature is the same as that of the gas flow, 296K. Considering that the singly charged fraction (positive or negative) is 34.4 % for 0.04 μm particles, the theoretical particle deposition efficiency due to image force for the particles in Boltzmann charge equilibrium is 0.019 % (Re=1600) or 0.020 % (Re=640). That is, the theoretical calculation also shows that the electrostatic effect does not increase the deposition efficiency for particles in Boltzmann charge equilibrium.

The deposition efficiency data show little difference between oleic acid and NaCl particles. That is, particle material has no effect on particle deposition efficiency. This is expected as the Knudsen number is greater than 3, the thermophoretic coefficient will remain constant at 0.55 and is independent of particle conductivity (Messerer et al., 2003). In this study, Kn ranges from 3.3 to 13.5. Therefore, tube wall temperature needed to completely suppress particle deposition of a given particle size is the same for different particle materials.

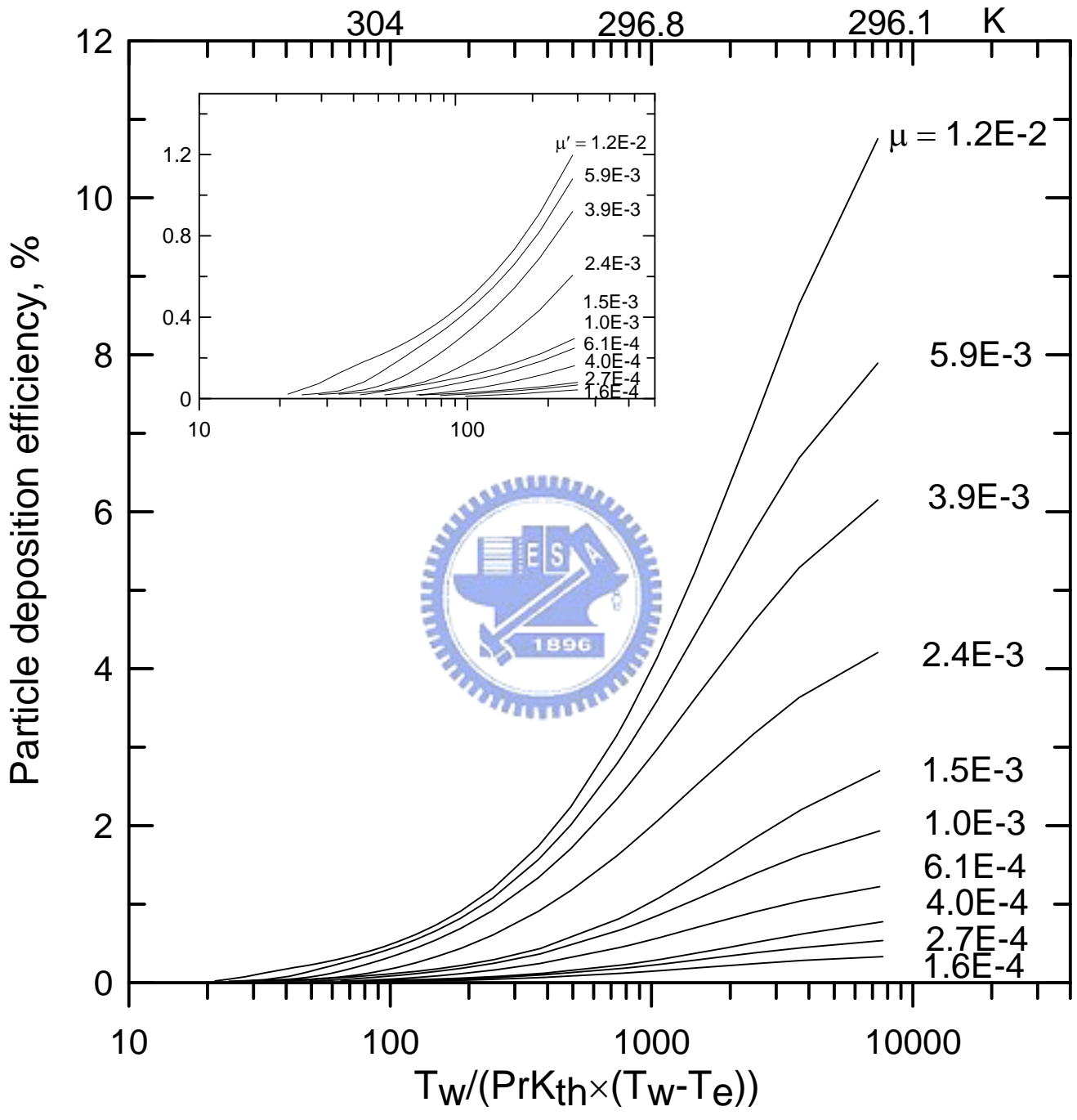
6.3 Particle deposition efficiency versus dimensionless temperature difference and deposition parameter

The particle deposition efficiency can be plotted as a function of the dimensionless temperature difference, $\theta = T_w / (\text{Pr}K_{th}(T_w - T_e))$, and laminar diffusional deposition parameter, $\pi DL/Q$, as shown in Figs. 6.4(a) and (b). The dimensionless temperature difference is the negative of the inverse thermophoretic parameter. The deposition parameter μ ranges from 1.6×10^{-4} to 1.2×10^{-2} and 1.2×10^{-2} to 1.16 in Figs. 6.4(a)-(b), respectively, to cover the entire range of μ' . It is shown that when μ' is small and less than 1.2×10^{-2} (Fig. 6.4(a)), the deposition efficiency is less than 11 %, in the range of dimensionless temperature difference (10-1000) studied. The deposition efficiency is seen to decrease monotonically to zero as the dimensionless temperature difference is decreased from 7600 to less than 70. Whereas in Fig. 6.4(b), when μ' ranges from 1.2×10^{-2} to 1.16, the deposition efficiency ranges from 0 to 100 %. It is seen that when μ' is larger and closer to 1, the particle deposition efficiency is decreased more sharply with an decreasing $T_w / (\text{Pr}K_{th}(T_w - T_e))$. Zero particle deposition is achieved when $T_w / (\text{Pr}K_{th}(T_w - T_e))$ is smaller than a certain value. To obtain the required dimensionless temperature difference for zero deposition

efficiency, wall temperature was gradually increased until the deposition efficiency was reduced below about 0.04 %, which was the smallest achievable efficiency in the current simulation. Then the simulation was ceased.

The radial thermophoretic and diffusional velocities of aerosol particles were calculated by evaluating the temperature and concentration gradients at the tube wall, respectively, at different axial positions, as shown in Figs. 6.5. For the parameter μ' in the figures, L is increased while D and Q are fixed. The diffusional velocity evaluated at the tube wall is seen to remain constant in the axial direction while the thermophoretic velocity curves are different for three different heated wall temperatures, and a higher wall temperature gives rise to a higher particle thermophoretic velocity. For a fixed $T_w/(\text{Pr}K_{\text{th}}(T_w-T_e))$, when the radial thermophoretic velocity is higher than the diffusional velocity, particles will not deposit on the tube wall. This normally occurs near the entrance or the front part of the tube, or when L is less than a certain value assuming Q and D are fixed. Beyond that, the gas flow is heated to a temperature close to the wall temperature, such that the thermophoretic velocity drops below the diffusional velocity and particle deposition will occur again. That is, if the entire tube is heated, thermophoresis is only effective to suppress particle deposition for a certain front section of the tube only. The effective length depends on the particle diameter, flow rate, and $T_w/(\text{Pr}K_{\text{th}}(T_w-T_e))$. For example in Fig. 6.5(a), when $T_w/(\text{Pr}K_{\text{th}}(T_w-T_e))$ is 79.5, 53.8 and 41.0, the zero deposition region corresponds to μ' values less than 3.1×10^{-3} , 5.0×10^{-3} and 7.2×10^{-3} , respectively. Similarly in Fig. 6.5(b), when $T_w/(\text{Pr}K_{\text{th}}(T_w-T_e))$ is 22.3, 25.2 and 29.1, the zero deposition region corresponds to μ' values less than 8.2×10^{-3} , 1.18×10^{-2} and 2.7×10^{-2} , respectively.

(a)



(b)

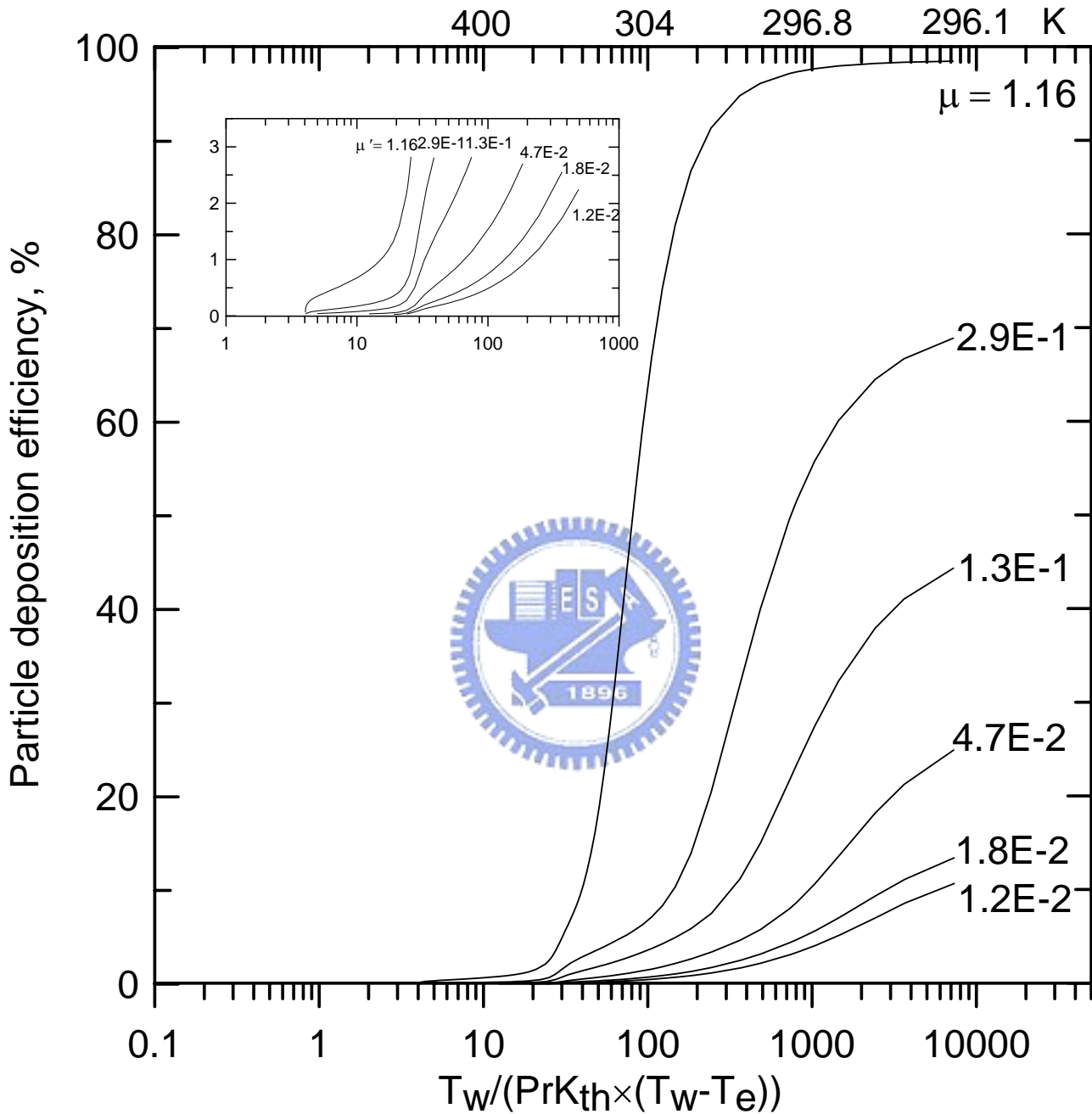


Figure 6.4 Particle deposition efficiency as a function of the dimensionless temperature difference, $T_w / (\text{Pr}K_{th}(T_w - T_e))$, and deposition parameter, $\pi DL/Q$. Dimensionless deposition parameter is (a) from 1.6×10^{-4} to 1.2×10^{-2} and (b) from 1.2×10^{-2} to 1.16. (Insets in the figures are deposition efficiency curves near zero deposition efficiency. For air and current tube geometry and length, the corresponding wall temperature is marked in the upper x-axis).

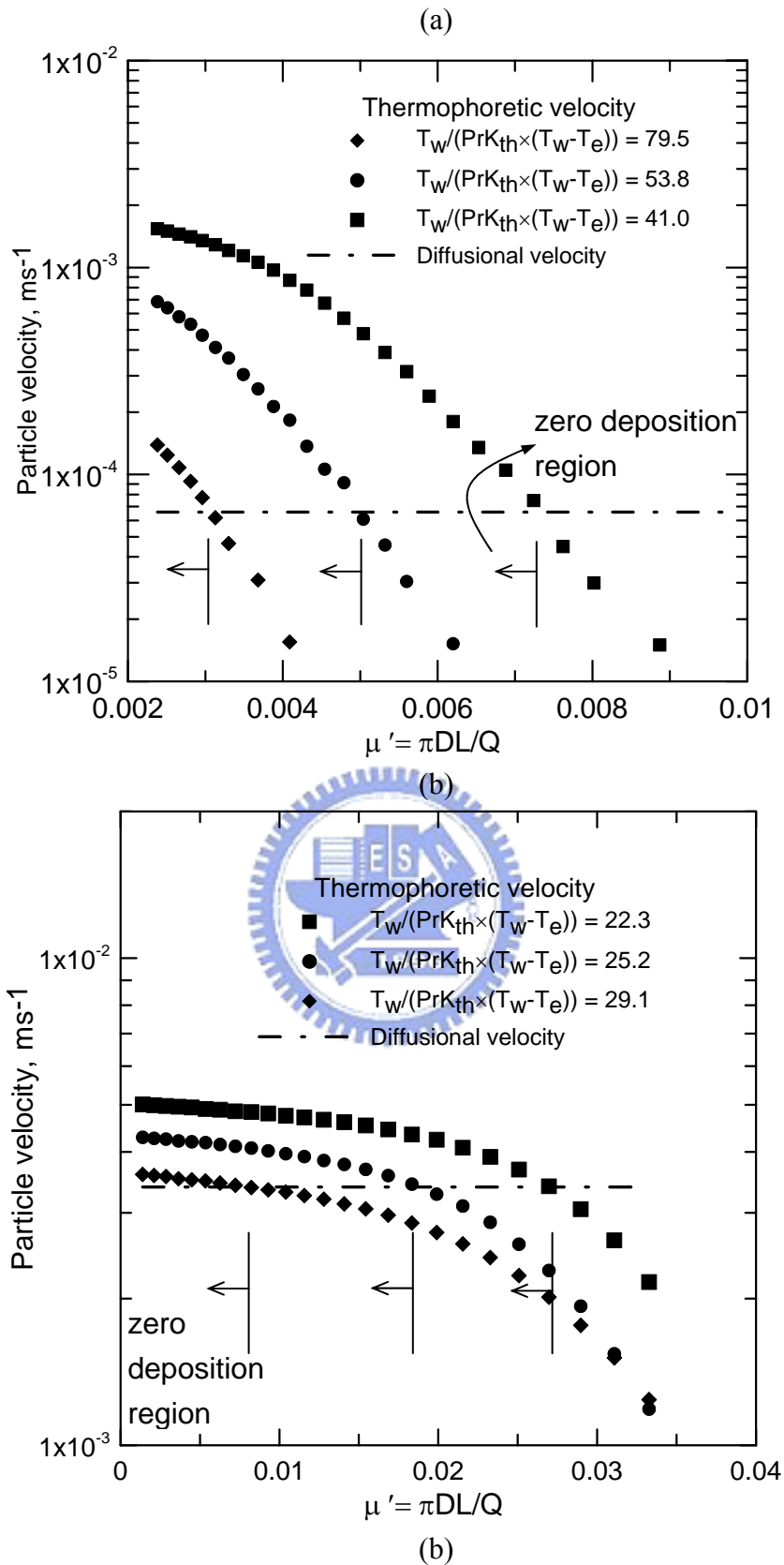


Figure 6.5 The variation of radial particle thermophoretic and diffusional velocities in the axial direction as the tube wall is heated at various temperatures at a given particle diameter of (a) $0.02 \mu\text{m}$ (b) $0.005 \mu\text{m}$ and a constant flow rate of 1 l min^{-1} .

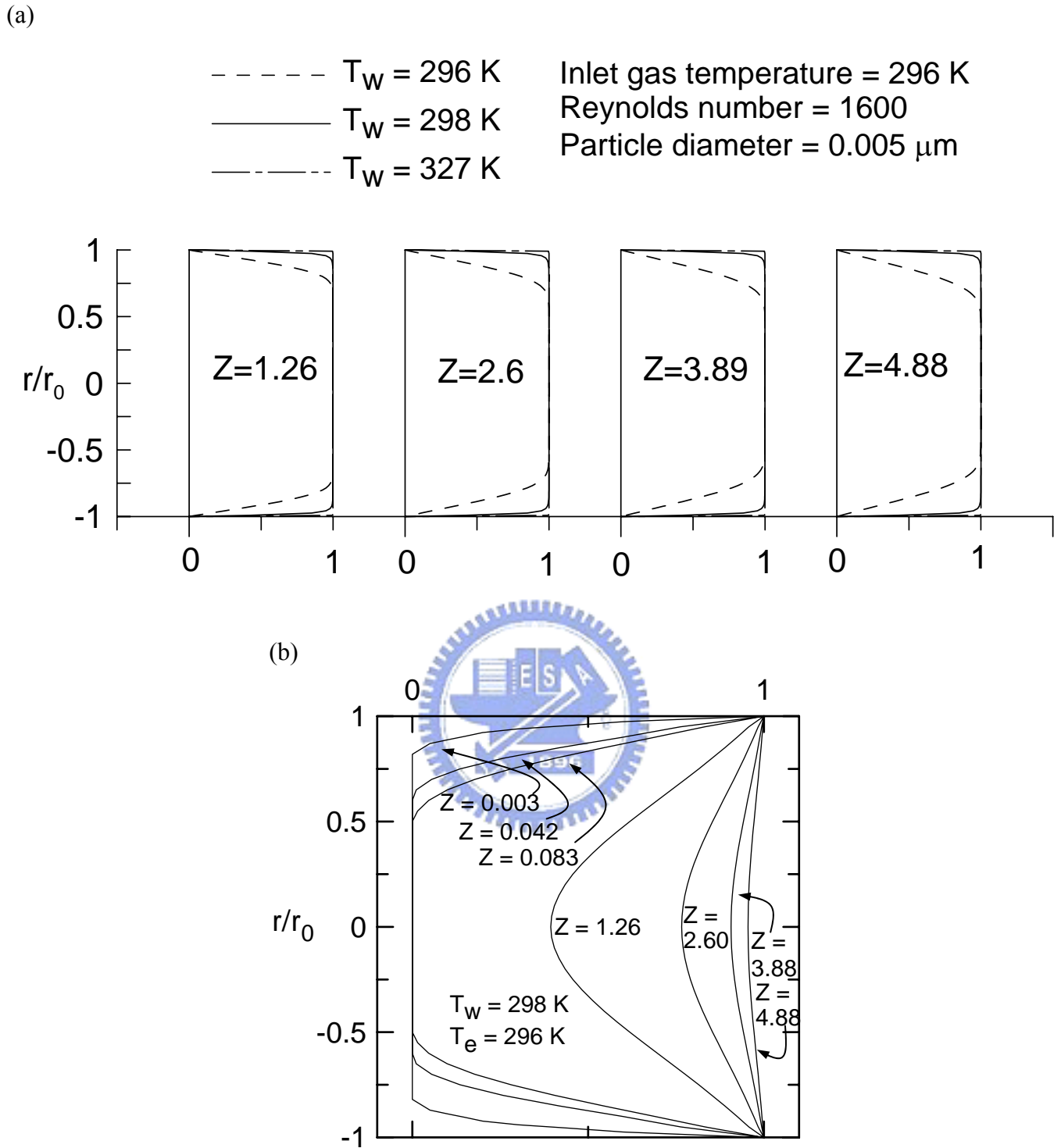


Figure 6.6 (a) Dimensionless radial concentration profiles and (b) dimensionless radial temperature profiles as a function of dimensionless axial coordinates. The test tube length and inside diameter are 1.18 and 0.0043 m, respectively.

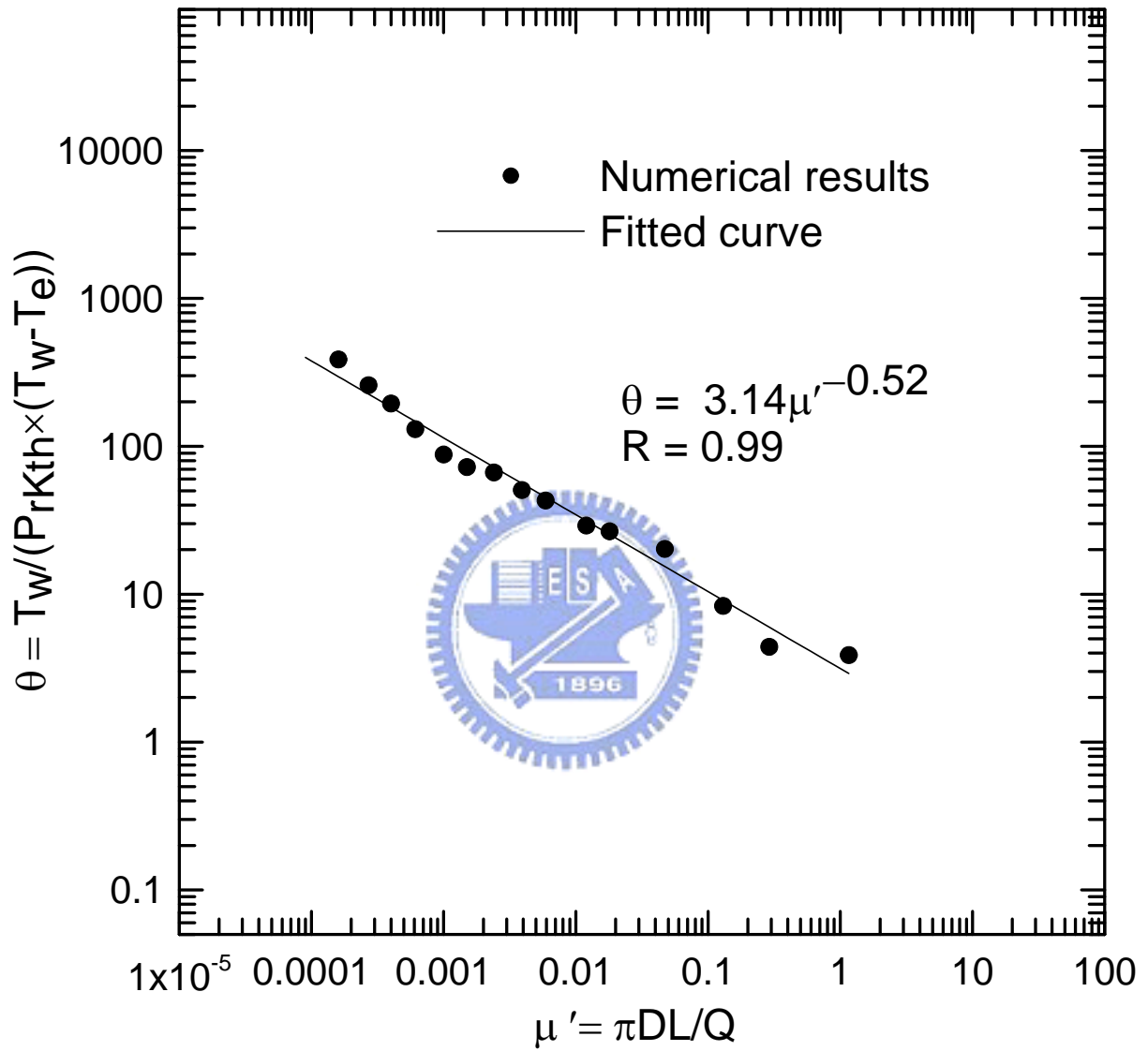


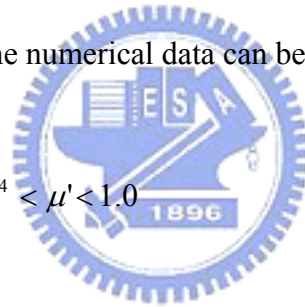
Figure 6.7 The relationship between the required dimensionless temperature difference, $\theta = T_w / (\text{Pr}K_{th}(T_w - T_e))$, and the dimensionless deposition parameter, $\mu' = \pi DL / Q$, for zero particle deposition for a circular tube air flow. Symbols represent the numerical results and solid line is the fitted curve.

Furthermore, as the temperature of the tube wall is heated slightly higher than that of the inlet gas flow, the radial concentration profiles along the axial direction can be shown to be quite different from the isothermal case. For example in the isothermal case, for a particle diameter of $0.005\ \mu\text{m}$, the convection-diffusion is strong and the deposition efficiency due to pure laminar diffusion is 28 % for the current tube geometry and length when $\mu' = 0.015$ (corresponding flow rate is 5 slpm, $\text{Re} = 1600$, tube ID is 0.0043 m, and length is 1.18 m). The dimensionless particle concentration profile near the wall is changed into more parabolic shape in an increasing dimensionless axial coordinate Z , as shown in Fig. 6.6(a). In contrast, when the tube wall is heated slightly higher than the inlet gas temperature by 2 K, the concentration profile has a much steeper slope near the wall and does not change very much in the axial direction. This dictates a constant concentration gradient and constant radial diffusional velocity (evaluated at the wall) in the axial direction as shown in Figs. 6.5. The deposition efficiency is also much smaller than the isothermal case. The wall temperature needed to suppress particle deposition completely is 327 K, and the corresponding dimensionless concentration profiles are also given in Fig. 6.6(a). The radial temperature profiles along the axial direction are shown in Fig. 6.6(b) when the tube wall is heated to 298 K. It can be seen that the temperature gradient is very high near the wall at the tube entrance and gradually decreases as the tube length increases. The high temperature gradient results in thermophoretic force that is high enough to overcome diffusional force and prevent particle deposition at the tube entrance. However, beyond a certain axial distance, the temperature gradient may drop below a value that is not high enough to suppress particle deposition.

6.4 An equation to predict the dimensionless temperature difference needed for zero particle deposition

A fitted equation to predict the dimensionless temperature difference needed for complete suppression of particle deposition can be obtained from the curve fitting of the present numerical results. The dimensionless temperature difference, $\theta = T_w / (\text{Pr} K_{th} (T_w - T_e))$, needed for zero deposition is plotted versus the dimensionless deposition parameter $\mu' = \pi DL/Q$, as shown in Fig. 6.7. The region below and to the left of the curve is the zero particle deposition region. It is seen that θ decreases (or T_w increases) sharply with respect to an increasing μ' (increasing diffusional strength). For example, θ is 343.4 when μ' is 1.2×10^{-4} and it drops to 120.5 when μ' is increased to 9.0×10^{-4} . The best fit to the numerical data can be expressed as

$$\theta = 3.14 \mu'^{-0.52}, \quad 1.6 \times 10^{-4} < \mu' < 1.0 \quad (6.1)$$



The above expression is useful for predicting the minimum wall temperature needed to achieve zero deposition efficiency in a laminar tube flow for any dimensionless deposition parameter. For example, for particles of $0.01 \mu\text{m}$ in diameter suspended in the tube flow with the flow rate of 0.5 slpm and inlet temperature of 320 K, the calculated μ' value is 6.1×10^{-3} for the present tube geometry and length (ID=0.0043 m, L=1.18 m). The θ value for complete suppression of particle deposition is 44.2, which corresponds to a minimum wall temperature of 340K.

6.5 Practical application

In semiconductor dry etching or CVD process, the exhaust pipe is usually heated to prevent particle deposition. The pipe diameter used is usually several inch in diameter for the exhaust of a vacuum pump. Taking a 2" tube for example, particles of $0.003\ \mu\text{m}$ in diameter suspended in the pipe flow ($L=5\ \text{m}$) with the flow rate of 85.0 slpm and inlet temperature of 353 K, the calculated μ' value is 6.43×10^{-3} . The θ value for complete suppression of particle deposition is 43.3, which corresponds to a minimum wall temperature of 374 K. While for particles of $0.005\ \mu\text{m}$ in diameter, the calculated minimum wall temperature is 365 K for zero particle deposition.



CHAPTER 7

CONCLUSIONS AND FUTURE STUDY

7.1 Conclusions

In the first part of this thesis, the effect of developing flow and temperature of a cylinder tube flow on the thermophoretic deposition efficiency was investigated numerically. It is found that by taking into account the effect of developing flow at the entrance region, a higher deposition efficiency is obtained than that of fully developed flow. Although the developing temperature gradients in the radial direction of developing temperature profiles are higher than those of fully developed temperature profiles at the entrance of a tube or the position of a temperature jump, the increase of deposition efficiency is almost negligible for a long tube, if the flow is fully developed. However, when both flow and temperature are developing, the deposition efficiency is significantly higher than the case of fully developed flow in which the fluid velocity, and hence the particle flux is zero near the wall. Equations are also developed empirically to predict the thermophoretic particle deposition efficiency in both the combined developing and combined fully developed cases under laminar flow conditions.

In the experimental study, thermophoretic particle deposition efficiencies in both laminar and turbulent tube flows were investigated and compared with the empirical expression of combined fully developed case developed in this study and the theoretical expression of Romay et al. (1998), respectively. The experimental results show that the deposition efficiency due to particle diffusion and particle electrostatic charge is comparable to thermophoretic deposition efficiency and should be excluded

so that one can obtain accurate experimental data for thermophoretic particle deposition efficiency. Even for particles in Boltzmann charge equilibrium, the deposition efficiency due to particle electrostatic charge is important when compared with the thermophoretic deposition efficiency. For particles that are completely charge neutral, the isothermal deposition efficiencies agree very well with the available theories in the literature, while the thermophoretic deposition efficiencies also agree very well with the theoretical expressions of Romay et al. (1998) in turbulent flow and empirical expression of combined fully developed case developed in laminar flow.

To prevent particle deposition in tube flow, a common method is to heat up the tube wall such that the temperature is higher than that of the gas flow. In the present study, suppression of particle deposition by thermophoresis in laminar tube flow was investigated numerically. Good agreement was obtained between the numerical results and experimental data. A sharp reduction of particle deposition efficiency occurs as the tube wall is heated to a temperature slightly higher than that of the gas flow. Complete suppression, or zero particle deposition is achieved when $T_w / (\text{Pr} K_{th} (T_w - T_e))$ is less than a certain value, which is determined solely by μ . The effective region to completely suppress particle deposition occurs near the front section of the tube where temperature difference still exists between the tube wall and the flow. Beyond that region, particle deposition occurs again when the flow is gradually heated in the axial direction to a certain temperature such that particle thermophoretic force is reduced below the diffusional force.

An empirical expression has been developed to calculate the dimensionless temperature difference, and hence the minimum wall temperature, needed for zero

particle deposition for a given dimensionless deposition parameter ranging from 1.6×10^{-4} to 1.0.

7.2 Future study

Thermophoretic particle deposition efficiency is investigated at 1 atm in this study. There are practical applications in the high-tech industry to prevent particle deposition in tube flow in vacuum. Thus, it is of great interest to investigate further the thermophoretic particle deposition in vacuum in the future.

There have been some developments in the filterless removal of combustion aerosol particles, such as diesel soots, by thermophoretic precipitator. Messerer et al. (2004) developed a miniature pipe bundle heat exchanger to enhance the particle collection efficiency. The experimental results show that collection efficiency is not high enough, and the deposited soot particles lead to enhanced isothermal deposition and reduced thermophoretic deposition after the long-term operation, a typical soiling effect. In the future, it is worthwhile to develop a highly efficient thermophoretic precipitator and investigate the effect of soiling on the thermophoretic particle deposition efficiency.

This study has shown that the present theories under-predict particle deposition efficiency by image force for particles in Boltzmann charge equilibrium. In the presence of external electric field, the deposition of charged particle can be enhanced further. Fan and Ahmadi (1993) investigated the particle deposition in turbulent flow numerically and develop an empirical equation for the non-dimensional deposition velocity enhanced by electrostatic. The numerical results show that the deposition

rate of particles $< 10 \mu\text{m}$ increases significantly as the electric field intensity increases. However, experimental validation of the empirical equation is not yet available. Further experimental study in the electrostatic effect on particle deposition is therefore necessary and warranted.



Appendix A: Derivation of equation for the combined fully developed case

Assuming steady, laminar fluid flow in a circular tube, thermophoretic velocity $V_{th}(r, z)$ in the radial direction is a function of r and z , and the particle equations of motion, Eqs. (2.8) and (2.9), can be simplified as

$$\frac{dr}{dt} = V_{th}(r, z) \quad (\text{A.1})$$

$$\frac{dz}{dt} = u(r) = 2u_m \left[1 - \left(\frac{r}{r_0} \right)^2 \right] \quad (\text{A.2})$$

The critical particle trajectory can be calculated by

$$\int_{r_c}^{r_0} \frac{dr}{V_{th}(r, z)} = \int_0^L \frac{dz}{u(r)} \quad (\text{A.3})$$



The temperature gradient in the radial direction can be found by the energy equation as

$$\frac{1}{r} \frac{d}{dr} \left(r \frac{dT}{dr} \right) = \frac{2u_m}{\alpha} \left(\frac{dT_m}{dz} \right) \left[1 - \left(\frac{r}{r_0} \right)^2 \right] \frac{T_w - T}{T_w - T_m} \quad (\text{A.4})$$

The mixing-cup temperature distribution is a function of z only and is given by Incropera and De Witt (1996) as

$$\frac{T_m(z) - T_w}{T_{in} - T_w} = \exp \left(- \frac{\pi D_t h z}{\rho Q C_p} \right) \quad (\text{A.5})$$

where $h = \frac{Nu_D \times k_g}{D_t}$ and Nu_D (Nusselt number) = 3.66 for the constant wall temperature condition.

Combing Eq. (A.5) and the invariant fully developed temperature profile, Eq. (2.4), Eq. (A.4) can be solved analytically to obtain the temperature gradient, and the corresponding thermophoretic velocity can be obtained as the product of two functions: $g(r)$ and $h(z)$, where $g(r)$ depends on r while $h(z)$ depends on z only. Taking separation of variable of equation (A.3) results in the following dimensionless analytical equation which can be solved to obtain the dimensionless critical radial position, R_c ,

$$\int_{R_c}^1 f(R) dR = -Pr K_{th} \ln \left(\frac{T_w}{T_e} + \left(\frac{T_e - T_w}{T_e} \right) \exp \left(\frac{-3.66\alpha L}{u_m r_0^2} \right) \right) \quad (A.6)$$

where $f(R) = \frac{1 - R^2}{0.903R - 0.0136R^2 - 1.323R^3 + 0.355R^4 + 0.581R^5 - 0.248R^6}$, and $R_c = r_c/r_0$ is the dimensionless critical radial position. Once R_c is obtained, thermophoretic particle deposition efficiency can be calculated.

REFERENCES

- Allen, M. D., and Raabe, O. G. (1985) Slip correction measurement of spherical solid aerosol particles in an improved Millikan apparatus. *Aerosol Sci. Technol.* 4, 269-286.
- Bae, G. N., Lee, C. S., and Park, S. O. (1995) Measurements and control of particle deposition velocity on a horizontal wafer with thermophoretic effect. *Aerosol Sci. Technol.* 23, 321-330.
- Baron, P. A., and Willeke, K. (2001) *Aerosol Measurement: Principles, Techniques and Applications*. John Wiley & Sons, New York, 174.
- Batchelor, G. K., and Shen, C. (1985) Thermophoretic deposition of particles in gas flowing over cold surface. *J. Colloid Interface Sci.* 107(1), 21-37.
- Brock, J. R. (1962) On the theory of thermal forces acting on aerosol particles. *J. Colloid Sci.* 17, 768-780.
- Chang Y. C., Ranade M. B., and Gentry J. W. (1995) Thermophoretic deposition in flow along an annular cross section: experiment and simulation. *J. Aerosol Sci.* 26, 407-428.
- Chiou, M.-C. (1996) Random eddy model for prediction of thermophoretic effects on particle deposition processes. *J. Chinese Soc. Mech. Engng.* 17(3), 281-288.

Cohen, B. S., Xiong, J. Q., Asgharian, B., and Ayres, L. (1995) Deposition of inhaled charged ultrafine particles in a simple tracheal model. *J. Aerosol Sci.* 26(7), 1149-1160.

Derjaguin, B. V., Rabinovich, Ya. I., Storozhilova, A. I., and Shcherbina, G. I. (1976) Measurement of the coefficient of thermal slip of gases and the thermophoresis velocity of large-size aerosol particles. *J. Colloid Interface Sci.* 57, 451-461.

Fan, B. J., Cheng, Y. S., and Yeh, H. C. (1996) Gas collection efficiency and entrance flow effect of an annular diffusion denuder. *Aerosol Sci. Technol.* 25, 113-120.

Fan, F. G., and Ahmadi, G. (1993) A sublayer model for turbulent deposition of particles in vertical ducts with smooth and rough surfaces. *J. Aerosol Sci.* 21, 49-71.

Friedlander, S. K., and Johnstone, H. F. (1957) Deposition of suspended particles from turbulent gas stream. *Ind. Engr. Chem.* 49, 1151-1156.

Friedlander, S. K. (2000) *Smoke, Dust, and Haze*, John Wiley & Sons, New York.

Grigull, U., and Tratz, H. (1965) Thermischer einlauf in ausgebildeter laminarer Rohrströmung. *Int. J. Heat Mass Transfer*, 8, 669-678.

He, C., and Ahmadi, G. (1998) Particle deposition with thermophoresis in laminar and turbulent duct flows. *Aerosol Sci Technol.* 29, 525-546.

Hinds, W. C. (1999) *Aerosol technology*, 2nd Ed., Wiley, New York.

Incropera, F. P., and De wit, D. P. (1996) *Fundamentals of heat and mass transfer*, Wiley, New York.

Kasper, G. (1981) Electrostatic dispersion of homopolar charged aerosols. *J. Colloid Interface Sci.* 81(1), 32-40.

Kays, W. M., and Crawford, M. E. (1993) *Convective heat and mass transfer*, 3rd ed., McGraw-Hill, New York.

Konstandopoulos, A., and Rosner, D. E. (1995) Inertial effects on thermophoretic transport of small particles to walls with streamwise curvature—I. Theory. *Int. J. Heat Mass Transfer* 38, 2305-2327.

Lee, B. U., and Kim, S. S. (2002) The effect of varying impaction plate temperature on impactor performance: experimental results. *J. Aerosol Sci.* 33, 451-457.

Lee, K. W., and Gieseke, J. A. (1994) Deposition of particles in turbulent pipe flows. *J. Aerosol Sci.* 25(4), 699-709.

Lin, C. S., Moulton, R. W., and Putnam, G. L. (1953) Interferometric measurements of concentration profiles in turbulent and streamline flow. *Ind. Eng. Chem.*, 45, 640-646.

Liu, B. Y. H., and Agarwal, J. K. (1974) Experimental observation of aerosol deposition in turbulent flow. *J. Aerosol Sci.* 5, 145.

Liu, B. Y. H., and Ahn, K. H. (1987) Particle deposition on semiconductor wafers. *Aerosol Sci. Technol.* 6, 215-224.

Messerer A., Niessner R., and Pöschl U. (2003) Thermophoretic deposition of soot aerosol particles under experimental conditions relevant for modern diesel engine exhaust gas systems. *J. Aerosol Sci.* 34, 1009-1021.

Messerer A., Niessner R., and Pöschl U. (2004) Miniature pipe bundle heat exchanger for thermophoretic deposition of ultrafine soot aerosol particles at high flow velocities. *Aerosol Sci. Technol.* 38, 456-466.

Nishio, G., Kitani, S., and Takahashi, K. (1974) Thermophoretic deposition of aerosol particles in a heat-exchanger pipe. *Ind. Engng Chem, Process Des. Develop.* 13(4), 408-415.



Patankar S. V. (1980) *Numerical heat transfer and fluid flow*, McGraw-Hill, New York.

Pich, J. (1978) Comments on the paper: C. P. Yu's Precipitation of unipolarly charged particles in cylindrical and spherical vessels. *J. Aerosol Sci.* 9, 275-278.

Rader, D. J., and Marple, V. A. (1985) Effect of ultra-Stokesian drag and particle interception on impaction characteristics. *Aerosol Sci. Technol.* 4, 141-156.

Rader, D. J. (1990) Momentum slip correction factor for small particles in nine common gases. *J. Aerosol Sci.* 21, 232-239.

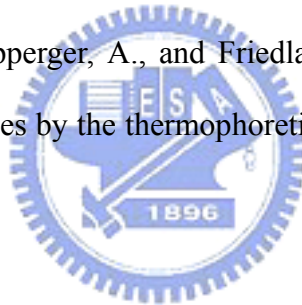
Romay, F. J., Takagaki, S. S., Pui, D. Y. H., and Liu, B. Y. H. (1998) Thermophoretic deposition of aerosol particles in turbulent pipe flow. *J. Aerosol Sci.* 29(8), 943-959.

Santachiara, G., Prodi, F., and Cornetti, C. (2002) Experimental measurements on thermophoresis in the transition region. *J. Aerosol. Sci.* 33, 769-780.

Skelland, A. H. P. (1974) *Diffusional mass transfer*, Wiley, New York.

Sparrow, E. M., Lin, S., and Lundgren, T. S. (1964) Flow development in the hydrodynamic entrance region of tubes and ducts. *Phy. Fluid* 7, 338-347.

Stratmann, F., Fissan, H., Papperger, A., and Friedlander, S. (1988) Suppression of particle deposition to surfaces by the thermophoretic force. *Aerosol Sci. Technol.* 9, 115-121.



Stratmann, F., Otto, E., and Fissan, H. (1994) Thermophoretic and diffusional particle transport in cooled laminar tube flow. *J. Aerosol Sci.* 25(7), 1305-1319.

Talbot, L., Cheng, R. K., Schefer, R. W., and Willis, D. R. (1980) Thermophoresis of particles in a heated boundary layer. *J. Fluid Mech.* 101(4), 737-758.

Tsai, C-J., and Lu, H-C. (1995) Design and evaluation of a plate-to-plate thermophoretic precipitator. *Aerosol Sci. Technol.* 22, 172-180.

Waldmann, L. (1961) In *Rarefied Gas Dynamics*, L. Talbot ed., Academic, New York, 323.

Walker, K. L., Homsy, G. M., and Geyling, R. T. (1979) Thermophoretic deposition of small particles in laminar tube flow. *J. Colloid Interface Sci.* 69(1), 138-147.

Weinberg, M. C. (1982) Thermophoretic deposition efficiency for a nonuniform inlet particle concentration. *J. Amer. Ceramic Soc.* 65, 638-641.

Ye, Y., Pui, D. Y. H., Liu, B. Y. H., Opiolka, S., Blumhorst, S., and Fissan, H. (1991a) Thermophoretic effect of particle deposition on a free standing semiconductor wafer in a clean room. *J. Aerosol. Sci.* 22, 63-72.

Ye, Y., Tsai, C. J., and Pui, D. Y. H. (1991b) Particle transmission characteristics of an annular denuder ambient sampling system. *Aerosol Sci. Technol.* 14, 102-111.

Yu, C. P., and Chandra, K. (1978) Deposition of charged particles from laminar flows in rectangular and cylindrical channels by image force. *J. Aerosol. Sci.* 9, 175-180.

Zoulalian, A., and Albiol, T. (1995) Analyse des interactions fluid-paroi dans un système ouvert a partir de la connaissance de la distribution des temps de séjour. Application aux dépôts d'aérosols par thermophorèse. *Canadian J. Chem. Engng.* 73, 800-807.

VITA

Name: Jyh-Shyan Lin

Date of Birth: October 12, 1976

Place of Birth: I-Lan Country, Taiwan, Republic of China

Education: 2000-2004 National Chiao Tung University, Ph. D. program in Institute of Environmental Engineering.

1998-2000 National Central University, M. S. program in Institute of Mechanical Engineering

1994-1998 National Central University, B. S. program in Department of Mechanical Engineering



作者：林智賢

出生地：台灣省宜蘭縣

出生日期：1976年10月12日

學歷：2000-2004 國立交通大學環境工程研究所博士班

1998-2000 國立中央大機械工程研究所碩士班

1994-1998 國立中央大機械工程學系

Publication list

A. Journal papers

1. **Lin, J. S.**, Tsai, C. J. and Chang, C. P. (2004) Suppression of particle deposition in tube flow by thermophoresis. *J. Aerosol Sci.* (accepted on 26 May 2004).
2. Tsai, C. J., **Lin, J. S.**, Aggarwal, S. G. and Chen, D. R. (2004) Thermophoretic deposition of particles in laminar and turbulent tube flows. *Aerosol Science and technology*. 38:131-139.
3. **Lin, J. S.** and Tsai, C. J. (2003) Thermophoretic deposition efficiency in a cylindrical tube taking into account developing flow at the entrance region. *J. Aerosol Sci.* 34:569-583.
4. Tsai, C. J., Lee, C. I., **Lin, J. S.**, and Huang, C. H. (2003) Control of particle reentrainment by wetting the exposed surface of dust samples, *Journal of the air and waste management association*. 53:1191-1195.
5. **Lin J. S.**, Tsai, C. J., Lin, H. and Chang, C. P. (2003) Field study on particle deposition in the exhaust pipeline of semiconductor manufacturing process. *Journal of Occupational Safety and Health*. (revised) (in Chinese)
6. Tsai, C. J., Huang, C. H., Liu, H. H. Cheng, Y. H. and **Lin, J. S.** (2003) A study of Nylon filter in adsorbing HCl and HNO₃ Gases. *Journal of Occupational Safety and Health*. 6 (11), 219-226 (in Chinese)

B. Conference papers (國際性)

1. **Lin, J. S.**, and Tsai, C. J. (2004) Study on thermophoretic deposition of aerosol particles in laminar and turbulent tube flows. Third Asia Aerosol Conference, Kowloon, Hong Kong, China (Oral presentation).
2. **Lin, J. S.**, and Tsai, C. J. (2003) Suppressing particle deposition by thermophoretic force in the pipe flow. 22th Annual AAAR Conference, Anaheim, California (Oral presentation).

3. **Lin, J. S.**, and Tsai, C. J. (2002) Thermophoretic deposition efficiency in laminar developing tube flow. 21th Annular AAAR Conference, Charlotte, North Carolina.
4. **Lin, J. S.**, and Tsai, C. J. (2002) Entrance effect on thermophoretic deposition efficiency. The sixth international aerosol conference, Taipei, Taiwan. (Oral presentation).
5. **Lin, J. S.**, Aggarwal, S. G. and Tsai, C. J. (2002) Suppression of particle deposition in tube flow by thermophoresis. The sixth international aerosol conference, Taipei, Taiwan.
6. Tsai, C. J., **Lin, J. S.** and Lin, H. (2002) Field study on particle deposition in the exhaust pipeline of semiconductor manufacturing process. The sixth international aerosol conference, Taipei, Taiwan.
7. Tsai, C. J., Lee, C. I., Huang, C. H. and **Lin, J. S.** (2002) Watering control for emission of particle reentrainment in a wind tunnel. The sixth international aerosol conference, Taipei, Taiwan.
8. Tsai, C. J., Huang, C. H., Cheng, Y. H., Lu, H. H. and **Lin, J. S.** (2002) Adsorption capacity of nylon filter for HCl and HNO₃ gases. The sixth international aerosol conference, Taipei, Taiwan.
9. **Lin, J. S.**, Tsai, C. J. and Chang, C. P. (2001) Theoretical thermophoretic and diffusional deposition efficiency of particles in cooled laminar tube flow. Second Asia Aerosol Conference, Pusan, Korea. (Oral presentation).

(國內)

1. **Lin, J. S.**, and Tsai, C. J. (2003) Thermophoresis effect on particle deposition efficiency in pipe flow. 2003 年氣膠科技研討會論文集，高雄，台灣。
2. 林宏、**林智賢**、蔡春進、張振平 (2002) 半導體製程廢氣管路中微粒沈降之實場研究。第一屆高科技工業環保技術及安全衛生學術及實務研討會論文集，新竹，台灣，第 101-110 頁，國立交通大學主辦。

3. **Lin, J. S.**, and Tsai, C. J. (2001) Theoretical thermophoretic deposition efficiency of aerosol particles in cooled turbulent tube flow. 第十八屆空氣污染研討會論文集，高雄，台灣。
4. **Lin, J. S.**, Tsai, C. J. and Chang, C. P. (2001) Theoretical thermophoretic and diffusional deposition efficiency of particles in cooled laminar tube flow. Oral presentation. 第九屆中華民國氣膠科技研討會論文集，雲林，台灣，第308-312頁。

C. Others

期刊論文

1. 江漢全、林智賢 (2002) 蘭陽平原農田土壤砷之分佈，宜蘭技術學報第九期工學專輯，第153~161頁。
2. Chiang, H. C., Hsiao, H. H., and **Lin, J. S.** (2001) Investigation on arsenic content in drinking water well samples in Lan-Yang Plain. Journal of Environmental Protection Society of the Republic of China, 24(1), 82-93. (in Chinese)
3. Lin, J. C., **Lin, J. S.** and Lee, S. L. (1999) Resistance to silver electrolytic migration for Ni-deposited Ag Thick-Film. Journal of Chinese Corrosion Engineering, 13(3), 111-116. (in Chinese)

研討會論文

1. **Lin, J. S.** and Lin, J. C (1999) Resistance to silver electrolytic migration for Ni-deposited Ag Thick-Film. 中華民國防蝕工程學會 88 年年度會員大會暨論文發表會論文集，南投，臺灣。

碩士論文

1. 林智賢 (2000) 鎳、銅表面鍍層對含銀厚膜之抗遷移性研究，國立中央大學機械工程研究所碩士論文